Dielectric, Ferroelectric, and Optical Properties

Susanne Hoffmann-Eifert, *Peter Grünberg Institute & JARA-FIT, Forschungszentrum Jülich, Germany*

Dieter Richter, *Jülich Centre for Neutron Science & Institute for Complex Systems, Forschungszentrum Jülich, Germany*

Susan Trolier-Mc Kinstry, *MATSE Department, Pennsylvania State University, USA*

Content

Dielectric, Ferroelectric, and Optical Properties

1 Introduction

Dielectric and ferroelectric materials historically have had and continue to have a strong influence on the evolution of today's electrical engineering, electronics, optics, and information technology. In this chapter, we will predominantly discuss the material class of crystalline oxides. In device applications, these materials are employed as bulk materials and, in nanoelectronic typically as thin films.

The range of new applications for these materials in the field of information technology is extremely wide. Low permittivity dielectrics are being developed as insulators on advanced CMOS circuits in order to enhance the signal transfer rate across the chips (Chap. 34). High permittivity dielectrics and ferroelectrics are being investigated for the cell capacitors of future DRAM and non-volatile FeRAM devices, respectively (Chap. 27). Very low losses and a specific temperature dependence of the dielectric properties are required for new microwave oscillator and filter applications (Chap. 36). A variety of gate dielectrics for field-effect transistors are being studied for applications in short-channel MOSFETs (Chap. 14), carbon-based FETs (Chap. 20), and ion-sensitive FETs for electronic noses (Chap. 41). Even thinner dielectrics are used in tunnelling barriers, for example, in Coulomb blockage devices (Chap. 16), some molecular electronic test systems, as well as in Josephson junctions for super-conducting logic circuits (Chap. 18) and in quantum computing systems (Chap. 25). Gradients of the refractive index are used in optical wave guides (Chap. 35). The electrically switchable anisotropy of the refractive index (i.e. the birefringence) is employed in LCDs (Chap. 43), as well as in optical switches and modulators for data communication (Chap. 35). Holographic memories (Chap. 32) are based on the photosensitivity (either photo refraction or photo absorption) of an optical storage material. Pyroelectric materials are used in IR imaging systems (Chap. 40) and piezoelectric films control the deflection of the cantilever in MEMS devices, for example for dedicated micro-mirror displays (Chap. 46).

The development and optimization of the materials themselves and the related processing technologies has enabled the technical use of electronic phenomena at ever higher electrical fields, smaller circuit dimensions, and for an increasing number of functions. The future evolution of information technology will depend crucially on the possibility, reproducibility, and perfection of the integration of these new oxide dielectrics with semiconductor components.

The present chapter will introduce the basic concepts of the interaction of the electromagnetic field with matter, as this is one of the key issues in understanding the principles of the design and operation of the new electronic and photonic devices. The description of dielectric, ferroelectric and optical properties given here mainly focuses on the requirements of subsequent chapters. For further details or a broader view of the topic, the reader is referred to comprehensive textbooks either on solid state physics in general (e.g. [1]–[7]), electronic materials (e.g. [8]–[10]), or specifically on dielectric (e.g. [11]–[14]), ferroelectric (e.g. [18]–[20]), and optical properties (e.g. [56]–[58]).

2 Polarization of Condensed Matter

Before we enter into the specific physical description, we will first provide definitions of the following terms, which will be used throughout this chapter:

Dielectrics are insulating materials that are used technically because of their property of polarization to modify the dielectric function of a vacuum, for example to increase the capacity (i.e. the ability to store charge) of capacitors. They do not conduct electricity due to the very low density of *free* charge carriers. Here, the electrons are *bound* to microscopic regions within the material, that is the atoms, molecules, or clusters.

Polarization is the separation of a positive and a negative charge barycenter of bound charges. If this separation is induced by an applied electric field, it is called *dielectric* polarization. If the separation is induced by an applied strain field, it is called *piezo-*

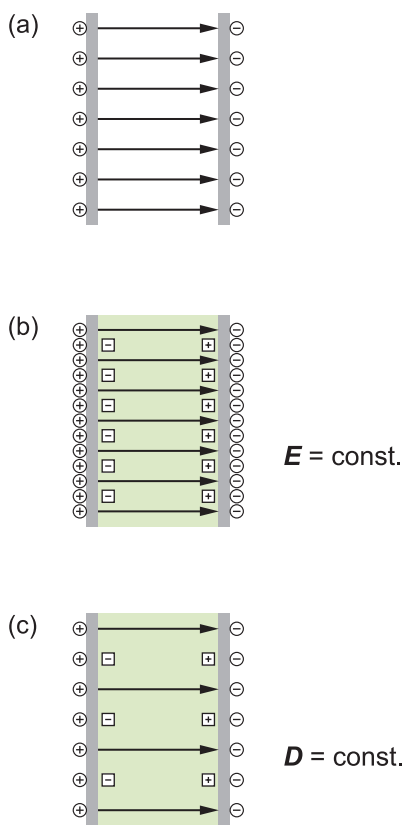

Figure 1:
(a) Empty parallel plate capacitor and
(b) capacitor after inserting a dielectric material between the electrode plates at constant voltage and
(c) at constant charge on the plates. Note: it is not necessary for the polarization $\boldsymbol{P}$ to be induced by the electric field $\boldsymbol{E}$.

electric polarization. Several dielectric crystals exhibit a *spontaneous polarization* below a critical temperature which is related to a change in crystal symmetry. A spontaneous polarization in the material leads to *pyroelectric* effects under temperature changes. *Ferroelectricity* is obtained when the orientation of polarization can be reoriented between crystallographically equivalent configurations by an external field.

Conductors such as metals conduct electric current because of the *free* mobility of the electronic charge carriers within their lattice. *Free* here means the charges can enter and leave a system in contrast to bound charges (or: polarization charges) which can only be displaced to a lesser or greater extent within the system.

Optical properties are determined by free and bound charges. The limiting cases of conductors (free conducting charges) and dielectrics (bound polarization charges) blend in the case of fields of high frequencies because here the charges are accelerated in only one direction during one half of a period of the alternating field and thus are unable to travel long distances.

2.1 Electrostatic Equations with Dielectrics

According to the **Poisson equation**, each *free* charge acts as a source for the dielectric displacement $\boldsymbol{D}$

$$\operatorname{div} \boldsymbol{D} = \rho_{\text{free}} \tag{1}$$

where ρ_{free} denotes the density of free (conducting) charges. Based on this relation, the overall charge neutrality of matter in an external field is described by

$$\boldsymbol{D} = \varepsilon_0 \boldsymbol{E} + \boldsymbol{P} \tag{2}$$

The term $\varepsilon_0 \boldsymbol{E}$ describes the vacuum contribution to the displacement $\boldsymbol{D}$ caused by an externally applied electric field $\boldsymbol{E}$, and $\boldsymbol{P}$ represents the electrical polarization of the matter in the system. Figure 1 illustrates the insertion of matter into a parallel plate capacitor. The effect on the dielectric displacement is independent of the cause of the polarization. The polarization may exist spontaneously (*pyroelectric*/*ferroelectric* polarization), it may be generated by mechanical stress (*piezoelectric* polarization), or it may be induced by an external electric field (*dielectric* polarization).

In the case of a **dielectric polarization**, the polarization of the matter is related to the electric field by

$$\boldsymbol{P} = \varepsilon_0 \chi_{\text{e}} \boldsymbol{E} \tag{3}$$

which leads to

$$\boldsymbol{D} = \varepsilon_0 \left(1 + \chi_{\text{e}}\right) \boldsymbol{E} = \varepsilon_0 \varepsilon_{\text{r}} \boldsymbol{E} \tag{4}$$

where χ_{e} defines the electrical susceptibility and ε_{r} the relative permittivity of the material.

2.2 Microscopic Approach and the Local Field

We are now going to find a correlation between the *macroscopic* polarization $\boldsymbol{P}$ and the *microscopic* properties of the material. The macroscopic polarization $\boldsymbol{P}$ is the vector sum of the individual *dipole moments* $\boldsymbol{p}$ of the material, such as polarized atoms, molecules, ions, etc.

$$\boldsymbol{P} = N_{\text{dip}} \cdot \boldsymbol{p} \tag{5}$$

with N_{dip} being the density of dipoles.

In the case of *dielectric* polarization, the dipole moments are induced by the local electric field $\boldsymbol{E}_{\text{loc}}$ at the site of the particle

$$\boldsymbol{p} = \alpha \cdot \boldsymbol{E}_{\text{loc}} \tag{6}$$

where α is the **polarizability** of an atomic dipole.

In condensed matter, the density and therefore the electrostatic interaction between the microscopic dipoles is quite high. Hence, the local field $\boldsymbol{E}_{\text{loc}}$ at the position of a particular dipole is given by the superposition of the applied field $\boldsymbol{E}_{\text{a}}$ and the field of all other dipoles

$$\boldsymbol{E}_{\text{loc}} = \boldsymbol{E}_{\text{a}} + \sum \boldsymbol{E}_{\text{dipole}} \tag{7}$$

The local field $\boldsymbol{E}_{\mathrm{loc}}$ can be calculated by the method of Clausius and Mossotti (see e.g. [6]). The calculation reveals a relation between the *atomic polarizability* α and the *macroscopic permittivity* ε_{r}. For example, for cubic crystal structures

$$\frac{N_{\mathrm{dip}}}{3\varepsilon_0}\,\alpha = \frac{\varepsilon_{\mathrm{r}} - 1}{\varepsilon_{\mathrm{r}} + 2} \tag{8}$$

is obtained. This is often referred to as the **Clausius-Mossotti equation**. It is important to remember that Eq. (8) has been developed only for induced dipoles (ionic and electronic polarization).

2.3 Mechanisms of Polarization

So far we have considered the correlation between the macroscopically measurable relative permittivity ε_{r} and the microscopic atomic polarizability α in an ensemble of induced dipoles. We will now extend our scope to both induced and permanent dipoles. In the following, the different physical mechanisms of polarization in the solid state will be outlined. Details can be found in textbooks such as reference [3].

In general, one can distinguish between four different types of polarization:

Electronic polarization describes the displacement of the negatively charged electron shell in relation to the positively charged nucleus. The electronic polarizability α_{el} is approximately proportional to the volume of the electron shell. Thus, large atoms have a large electronic polarizability. The temperature dependence of α_{el} can be neglected.

Ionic polarization is observed in materials with ionic bonds (i.e. ionic crystals) and describes the mutual displacement of the positive and negative sub-lattices under the influence of an applied electric field. In general, the temperature dependence of the ionic polarisability α_{I} is weakly positive because of the thermal expansion of the lattice.

Orientation polarization describes the alignment of permanent dipoles. Many substances contain molecules – either regular constituents or impurities – which carry a (permanent) electric dipole moment. If these dipoles are mobile or, at least, are able to reorient themselves by rotation, they contribute to dielectric polarization by the so-called orientation polarization. At ambient temperatures, usually all dipole moments are mutually compensated because of the orientation disorder. An electric field generates a preferred direction for the dipoles, while the thermal movement of the atoms perturbs the alignment. The average degree of orientation therefore is a function of the applied field and the temperature. The solution is given by the *Langevin function* [6]. For all technically applicable cases, the polarization is far from saturation and is proportional to the applied field. In this case, the average polarisability originating from permanent dipole moments $\boldsymbol{p}$ is given by

$$\left\langle \alpha_{\mathrm{or}} \right\rangle = \frac{p^2}{3\,k_{\mathrm{B}}T} \tag{9}$$

where k_{B} denotes the Boltzmann constant and T the absolute temperature measured in Kelvin. The strong temperature dependence is a main characteristic of the orientation polarisation.

Space-charge polarization describes a polarization effect in a dielectric material which shows spatial inhomogeneities of charge carrier densities. Space-charge polarization effects are not only of importance in semiconductor field-effect devices (see reference [7]), they also occur in ceramics with electrically conducting grains and insulating grain boundaries (so-called Maxwell-Wagner polarization, see reference [9]).

2.4 The Complex Dielectric Permittivity

We will now look at the behavior of dielectric material in alternating electric fields. Moving charges cause a frequency-dependent phase shift between applied field and charge displacement. To express this mathematically, the *relative dielectric permittivity* is written as a complex function

$$\underline{\varepsilon}_{\mathrm{r}} = \varepsilon_{\mathrm{r}}' + i\,\varepsilon_{\mathrm{r}}'' \tag{10}$$

The real part $\varepsilon_{\mathrm{r}}'$ characterizes the displacement of the charges, and the imaginary part $\varepsilon_{\mathrm{r}}''$ the dielectric losses. Analogously, the *electrical susceptibility* is also written as a complex quantity

$$\underline{\chi}_{\mathrm{e}} = \chi_{\mathrm{e}}' + i\chi_{\mathrm{e}}'' \tag{11}$$

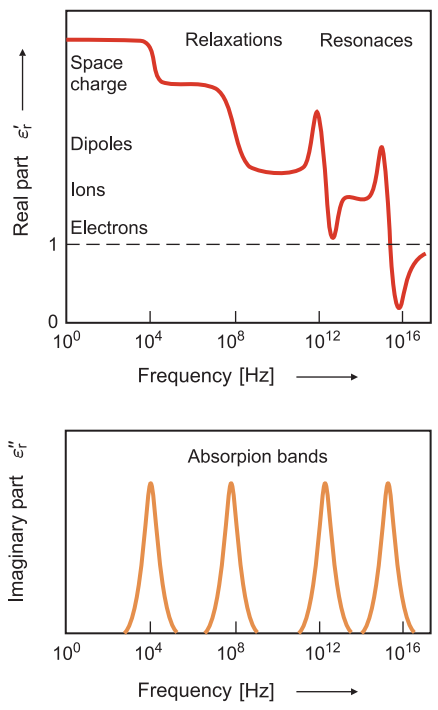

Figure 2: Frequency dependence of real (top) and imaginary (bottom) part of the dielectric function.

The **loss tangent** is defined as

$$\tan\delta \equiv \frac{\varepsilon_r''}{\varepsilon_r'} \tag{12}$$

In addition to the losses caused by dipole reorientation $(\tan\delta)_{\text{dipole}}$, the residual leakage current $(\tan\delta)_{\text{cond}}$ of the non-perfect insulator is added, so that in general $\tan\delta$ and hence ε_r'', respectively, become the sum of both contributions

$$\tan\delta = (\tan\delta)_{\text{dipole}} + (\tan\delta)_{\text{cond}} \tag{13}$$

For microwave ceramics (see Chap. 36), a quality factor $Q := \tan^{-1}\delta$ is frequently quoted.

The total polarization of a dielectric material originates from the four contributions discussed above. Each contribution stems from a short-range movement of charges responding to an electric field on different time scales and, hence, through a Fourier transform, in different frequency regimes. The resulting dispersion of the real and imaginary part of the dielectric function is shown in Figure 2.

The space-charge polarization is caused by a drift of mobile ions or electrons which are confined to outer or inner interfaces. Depending on the local conductivity, the space-charge polarization may occur over a wide frequency range from mHz up to MHz. The polarization due to the orientation of electric dipoles takes place in the frequency regime from mHz in the case of the reorientation of polar ligands of polymers up to a few GHz in liquids such as water. It is often possible to distinguish between space-charge and orientation polarization because of the temperature dependence of $\langle\alpha_{\text{or}}\rangle$. In the infrared region (10^{12}–10^{13} Hz), we find the resonance of the molecular vibrations and ionic lattices constituting the upper frequency limit of the ionic polarization. The resonance of the electronic polarization is around 10^{15} Hz. It can be investigated by optical methods. As can be seen from Figure 2, the different polarization mechanisms not only take place on different time scales but they also exhibit different frequency dependences. Depending on whether the oscillating masses experience a restoring force or not, we distinguish between resonance effects and relaxation effects, respectively. **Resonance** effects are observed for the ionic and electronic polarization, while **relaxation** effects are found for orientation polarization and space-charge polarisation.

2.5 Spontaneous Polarization

The ability of a crystal to exhibit spontaneous polarization is related to its symmetry. Following Maxwell's equations, spontaneous polarization is connected with surface charge density

$$P_s = Q_s / A \tag{14}$$

where (Q_s/A) is the density of surface charges.

2.5.1 Ferroelectricity

Ferroelectric materials exhibit a spontaneous polarization $\boldsymbol{P}_s$ which can be reoriented between two crystallographically equivalent configurations by an external field. Thus, it is not the existence of spontaneous polarization alone, but its reorientability by an external field which defines a ferroelectric material. The graph in Figure 3 displays a characteristic **hysteresis loop** occurring during the reversal of the polarization in a ferroelectric.

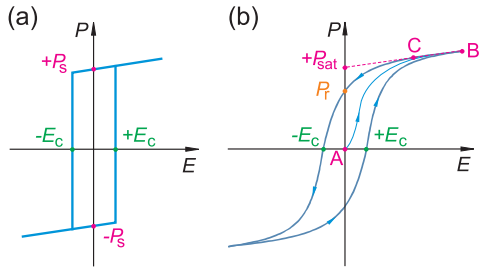

Figure 3: Hysteresis of the polarization P as a function of the field E for ferroelectric materials:
(a) Single-domain single crystal recorded in the polar direction. The remanent polarization P_r and the spontaneous polarization P_s are identical. An electrical field amplitude $E > E_c$ is needed to reverse the polarization.
(b) Polycrystalline sample. The line A-B gives the initial polarization curve. Extrapolation of the line B-C towards zero electric field gives the saturation polarization P_{sat} at $E = 0$. The hysteresis curve cuts the P axis at $E = 0$ giving the remanent polarization P_r. In order to reduce the polarization to zero, a coercive field $(-E_c)$ is necessary.

In the case of an ideal single crystal, the polarization vs. field behavior, P-E, can be explained by a simple superposition of two contributions: firstly, the dielectric, ionic and electronic polarization and, secondly, the *spontaneous polarization*, which is reoriented when the electric field E applied opposite to the polarization exceeds the coercive field E_c leading to the unidirectional jumps in the P-E curve. In polydomain ferroelectric materials, especially in ceramics, initially there is a statistical distribution of domains before the material is polarized for the first time. Starting with a polarization $P = 0$, P increases with an increasing field until it reaches saturation. The saturation polarization P_{sat} is obtained by extrapolating the graph to $E = 0$. If after saturation, the electric field is reduced again, then at $E = 0$, a remanent polarization P_r is found. P_r relates to the domain structure in the material. In order to bring the polarization to zero, a negative electric field of the magnitude of the coercive field E_c has to be applied. If the negative field is further increased, then the hysteresis loop is followed in the reverse sense.

As an illustration of the types of properties demonstrated by many ferroelectric materials, **barium titanate**, $BaTiO_3$, will be considered. The elementary cell is depicted in Figure 4. The **phase transition** in barium titanate is first order in character, and as a result, there is a discontinuity in the spontaneous polarization, spontaneous strain, and many other properties, as becomes clear in Figure 5. It is also obvious from Figure 5 that there are three phase transitions in $BaTiO_3$. In all cases, a small thermal hysteresis of the transition temperature is obtained, which depends on many parameters such as the rate of temperature change, mechanical stresses, crystal imperfections, etc. At the first transition upon cooling from high temperatures, at 123 °C, the system transforms from a *cubic* to a *tetragonal structure* with a spontaneous polarization in the [001] direction as shown in Figure 5a. The abrupt change of the spontaneous polarization of $\Delta P_s = 18\ \mu C/cm^2$ at the cubic-to-tetragonal transition temperature (see Figure 5c) clearly demonstrates a first-order phase transition. The second phase transition, at 5 °C, transforms the tetragonal structure to an *orthorhombic structure*. In this case, the polarization direction is in the [101] direction of the prototype cubic cell. Finally, at −90 °C, a further phase transition takes place which deforms the orthorhombic to a *rhombohedral structure*. There, the polarization is in the [111] direction. From a crystal chemical perspective, this series of phase transitions can be viewed as a consequence of the Ti^{4+} ion being somewhat too small to occupy the interstice created by the Ba-O framework. As a result, the series of phase transitions takes place to reduce the Ti cavity size [22].

Figure 5d displays the temperature dependence of the permittivity in barium titanate over the full temperature range. We note that the optical properties of ferroelectric materials are characterized by **birefringence**. $BaTiO_3$ is isotropic only in the cubic phase. The tetragonal and the rhombohedral phases are uniaxially birefringent, while the orthorhombic phase exhibits birefringent behavior with two axes.

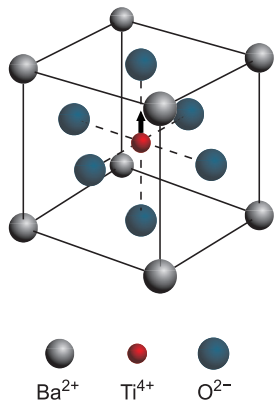

Figure 4: Unit cell of cubic $BaTiO_3$ (perovskite structure). The central Ti^{4+} ion is surrounded by six O^{2-} ions in octahedral configuration. The arrow schematically indicates one of the possible displacements of the central Ti^{4+} ion at the transition to the tetragonal ferroelectric structure that leads to a spontaneous polarization and, hence, to the ferroelectricity of tetragonal $BaTiO_3$ [21]. In reality, all ions are displaced against each other.

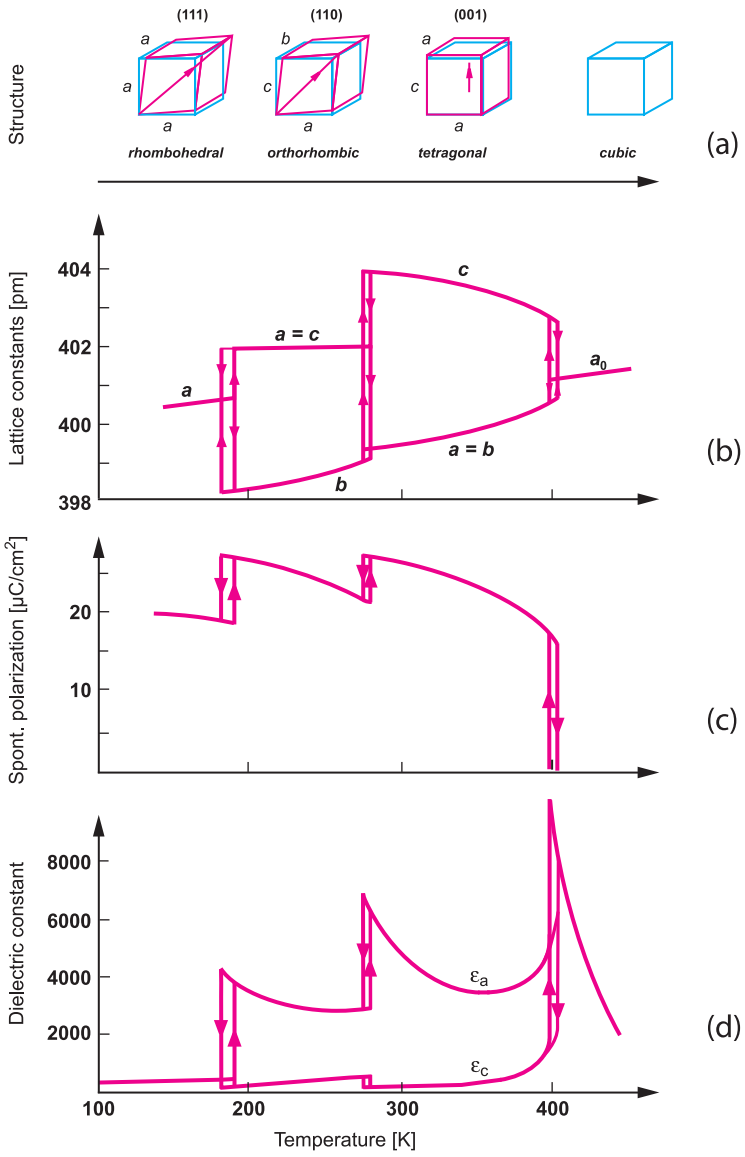

Figure 5: Various properties of $BaTiO_3$ as a function of temperature. Anisotropic properties are shown with respect to the lattice direction.
(a) Structure
(b) Lattice constants
(c) Spontaneous polarization P_s
(d) Relative permittivity ε_r

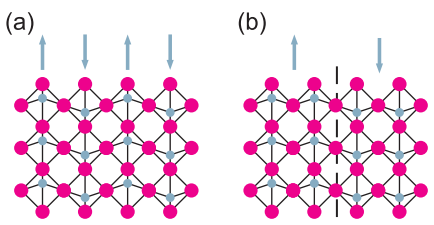

Figure 6: Sketch of perovskite structures. The red circles present the O^{2-} lattice, the grey dots the sublattices with positive charges.
(a) antiferroelectric structure,
(b) two oppositely polarized ferroelectric domains.

2.5.2 Antiferroelectricity

As in the case of magnetism, the electric dipole moments orient themselves in a parallel or antiparallel fashion. Figure 6 displays schematically two different polarization patterns. In Figure 6a, positively and negatively charged ions are displaced alternately in the downward and upward direction. The associated dipoles create an *antiferroelectric order*. Functionally, a material is referred to as antiferroelectric if it can be field-forced to a ferroelectric state (i.e. the free energies of the ferroelectric and antiferroelectric states must be similar). In contrast to this case, Figure 6b displays the behavior of the displacements close to a domain wall of a ferroelectric phase. Whether a given structure forms a ferroelectric or **antiferroelectric order** depends on the overall lattice forces and dipolar interactions [23].

Figure 7 displays the polarization dependence on the electric field in an antiferroelectric crystal. With a low electric field, a weak polarization is exhibited. Only if a critical field E_c, which breaks the antiferroelectric order is surpassed, will a major polarization occur. Around this critical field, hysteresis effects are observed in a similar way to those that occur in ferroelectric materials around $E = 0$ (see Figure 3), although in this case, the hysteresis is due to the field forcing a phase transition from the antiferroelectric to a ferroelectric phase. An example of an antiferroelectric is the material lead zirconate ($PbZrO_3$).

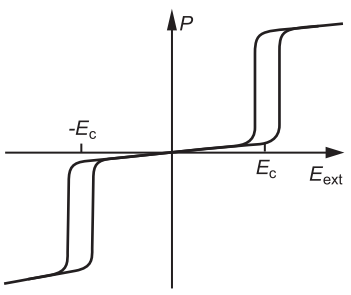

Figure 7: Antiferroelectric hysteresis loop. For $|E_{ext}| > E_c$ the system transforms into a ferroelectric state.

2.5.3 Pyroelectricity

The polarization charges of the surface of polar materials are usually screened by free charges causing residual currents (since no material has infinite resistivity) or charges captured from the ambient if the polar sample has been resting at a given temperature for some time.

However, since the *spontaneous polarization*, P_s, is temperature-dependent, any temperature change ΔT at a rate larger than the reciprocal time constant of the screening process will lead to uncompensated polarization charges

$$\Delta P = p_{py} \cdot \Delta T \tag{15}$$

where p_{py} denotes the **pyroelectric coefficient**.

These temporal changes in the surface charge $\Delta Q_s = \Delta P \cdot A$ can be electrically detected as a current, I, in an external circuit if electrodes (of area A) are attached to the polar material (see Figure 8). Some infrared detector arrays operating at room temperature are based on integrated pyroelectric materials (see Chap. 40).

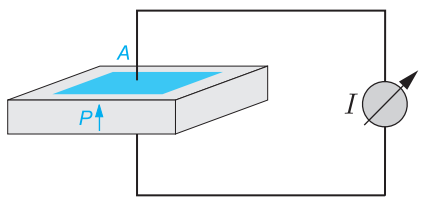

Figure 8: Slab of a pyroelectric crystal with the polarization vector and electrodes shown. A temperature change will lead to a current I.

2.5.4 Piezoelectricity

All polar crystals show piezoelectricity, since any **mechanical stress** $\boldsymbol{T}$ will result in a **strain** $\boldsymbol{S}$ because of the elastic properties of the material. The strain will affect the polarization since the polarization is caused by a displacement of the charge centres of the anions and cations. For small changes of the stress $\boldsymbol{T}$, the relation

$$\boldsymbol{P} = \boldsymbol{d} \cdot \boldsymbol{T} \tag{16}$$

is called the **direct piezoelectric effect**, where $\boldsymbol{d}$ denotes the tensor of the piezoelectric coefficients. The piezoelectric property of polar materials also leads to a **converse effect**: if an external electrical field, $\boldsymbol{E}$, is applied, a strain

$$\boldsymbol{S} = \boldsymbol{d}^t \cdot \boldsymbol{E} \tag{17}$$

is observed where the superior "t" denotes the transposed matrix. Note that the piezoelectric coefficients for the direct and the converse piezoelectric effect are thermodynamically identical. The strain response on an applied field shows the characteristic "butterfly loop" which is depicted in Figure 9 (see also [18]).

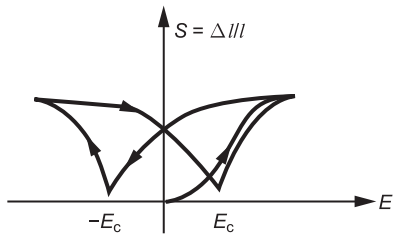

Figure 9: Schematic of the converse piezoelectric effect: characteristic "butterfly loop" of the strain S in dependence on the applied field E (the polarization P dependence is depicted in Figure 3)

The direct piezoelectric effect is employed for mechanical sensors, while the converse effect is used for mechanical actuators. In general, $\boldsymbol{P}$ and $\boldsymbol{E}$ are vectors, and $\boldsymbol{S}$ and $\boldsymbol{T}$ are second-rank tensors, resulting in third-rank tensors for the *piezoelectric coefficient*s d. The huge number of components of this tensor is significantly reduced for simple symmetries. For a material with a symmetry of infinity m, for example of poled ferroelectric ceramics, only three different d components remain. These are depicted in Figure 10:

- the *parallel component* d_{33} (Figure 10a) for a polarization if a stress is applied in the same direction or for a strain if the electric field is acting in the same direction;
- the *perpendicular component* d_{31} (Figure 10b) for a polarization if a stress is applied in perpendicular direction or for a strain if the electric field is acting in perpendicular direction.

- the *shear component* d_{15} (Figure 10c) for a dielectric displacement (polarization) if a shear stress is applied or for a shear strain if the electric field is acting.

The matrix notation for the *d* coefficients is described in detail in [24]. Both the parallel and the shear effect are employed in the piezoresponse mode of the AFM technique (see Chap. 31).

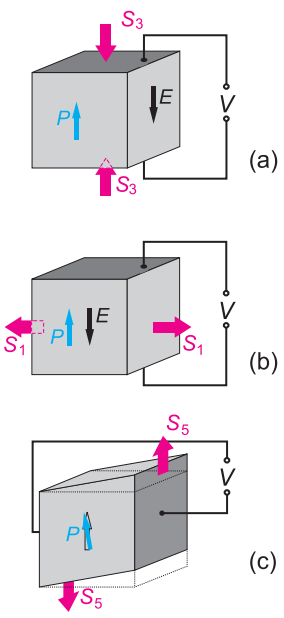

Figure 10: Three different configurations for determination of the tensor elements of the piezoelectric coefficient for a material with symmetry infinity m, for example a poled ferroelectric ceramic. The piezoelectric sample deforms under an applied electric field as a consequence of the converse piezoelectric effect. The tensor elements represent the directions of the applied electric field and measured strain response:
(a) parallel component d_{33},
(b) perpendicular component d_{31}, and
(c) shear component d_{15}.

3 Polarization Waves in Ionic Crystals

Having covered polarization phenomena at low frequencies, we will now look at the properties of polar dielectrics at higher frequencies.

The properties of dielectrics at frequencies from the microwave regime to the terahertz region ($\sim$ 1 GHz to $\sim$ 10 THz) are particularly dependent on the ionic polarization, whereas the optical properties ($f \geq 10^{14}$ Hz) are determined by electronic polarization. In Sec. 2.3, we described how electric fields displace the ionic sub-lattices and the electronic shell, thus creating induced polarization. In this section, we focus on the nature of these lattice oscillations and, after the introduction of some basic concepts, we will discuss the characteristic oscillations of technically relevant perovskites, such as strontium titanate or barium titanate.

3.1 Acoustic and Optical Phonons

Waves that can propagate in a crystal lattice are characterized by wave vectors $\boldsymbol{q}$, which can be reduced to the first **Brillouin zone** of the reciprocal lattice [16]. Therefore $\boldsymbol{q}$ has a value between zero and π/a (a: lattice constant).

In a three-dimensional **primitive lattice**, every $\boldsymbol{q}$-vector fits three lattice vibrations with different frequencies belonging to two **transverse** and one **longitudinal** branch of the **acoustic phonons** (see Figure 11). In the limiting case of long wavelengths, the acoustic phonons represent the macroscopic **sound waves** in the crystal. The dispersion of these waves is described by the sound velocity v_s: $\omega = v_s \cdot q$. For low frequency sound, the **group velocity** ($d\omega/dq$) is equal to the **phase velocity** (ω/q). Acoustic waves in the lattice cannot be excited directly by an electromagnetic wave. The reason is that the sound velocity is much lower than the velocity of light ($v_s \ll c_0$), and thus for a given angular frequency ω, one cannot find a sound wave with the same value of q as the periodicity of the electromagnetic wave. An indirect coupling of these waves is possible, however, for example in piezoelectric crystals [10].

In **non-primitive** lattices, the different atoms of the elementary cell can vibrate against each other, thus allowing frequencies $\omega \neq 0$, also in the case of $q = 0$. These are the characteristic vibrations, which are also called **optical phonons**. The opposite movement of neighboring atoms generates strong electric dipoles as soon as the atoms have non-equal electronegativities, that is their chemical bonds show some polar character. These phonons are described quantitatively by an effective charge Q^*, which defines the dipole moment $\boldsymbol{p} = Q^* \cdot \boldsymbol{u}$. This permits a strong coupling to electromagnetic waves (see Sec. 3.2).

For a basic understanding of the acoustic and optical phonons, we will discuss a simple model. A fundamental discussion of the properties of phonons can be found in the literature (e.g. [13]–[15]). In the limiting case of long wavelengths, a lattice with two kinds of atoms can be simplified by a linear chain of periodically arranged atoms A and B (compare Figure 12). The atoms are connected to their neighbors by small springs repre-

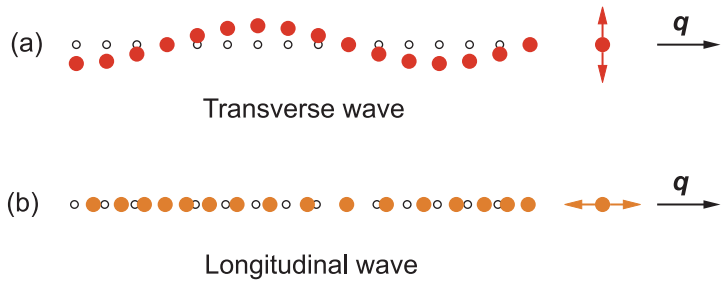

Figure 11: Different types of elastic waves in condensed matter:
(a) transverse wave and
(b) longitudinal wave.
The equilibrium positions of the atoms are marked by small circles.

senting the linear restoring force due to the chemical bond within the lattice. In this model, an oscillation of a single atom can spread over the whole crystal due to the connecting springs. This represents a system of **coupled harmonic oscillators**. The two types of atoms have masses of m_A and m_B, and at equilibrium they are separated by a distance $a/2$ along the x-axis. The crystal is periodic with a lattice constant of a. To calculate the deflection of the atoms, we set up a system of coupled differential equations that can be solved with the ansatz of plane waves.

The solution yields a **dispersion equation**, that is a relation between the angular frequency ω and the wave number q with two different values ω_+ and ω_- belonging to every q, as

$$\omega_{\pm}^2(q) = \frac{k}{\mu}\left[1 \pm \sqrt{1 - \frac{4\mu}{m_A + m_B} \cdot \sin^2\left(\frac{q\,a}{2}\right)}\right] \tag{18}$$

where k denotes the force constant of the connecting springs, and $\mu = (m_A m_B)/(m_A + m_B)$, the reduced mass of the vibrating system.

The two solutions $\omega_{\pm}(q)$ are plotted in Figure 13. They belong to different types of oscillations that show fundamentally different dispersion curves. The **optical branch** ($\omega_+(q)$) shows only a weak dependence of q and has its maximum frequency at $q = 0$. In contrast to this, at $q = 0$ the **acoustic branch** ($\omega_-(q)$) has the frequency $\omega_-(0) = 0$. The underlying oscillations are shown in Figure 12. Consecutive atoms are deflected in the same direction in the acoustic mode and in opposite directions in the case of optical oscillation.

In general, a lattice consisting of N atoms in the elementary cell can vibrate with $3N$ characteristic oscillations in three-dimensional space. *Three* of the vibrations are simple displacements of the elementary cell as a whole corresponding to the **acoustic phonons**. The remaining $3(N-1)$ vibrations belong to the **optical phonons**.

Two types of phonons can be distinguished differing with respect to the direction of the deflection $\boldsymbol{u}$ relative to the propagation vector $\boldsymbol{q}$. These are

- the *longitudinal phonons* characterized by $\boldsymbol{u} \parallel \boldsymbol{q}$, and
- the *transverse phonons* described by $\boldsymbol{u} \perp \boldsymbol{q}$.

In the case of the *pure elastic forces* considered here, the longitudinal optical and the transverse optical oscillations are degenerated. This degeneracy is removed in most cases since the local field $\boldsymbol{E}_{loc}$ caused by the neighboring atoms interacts with the polarization.

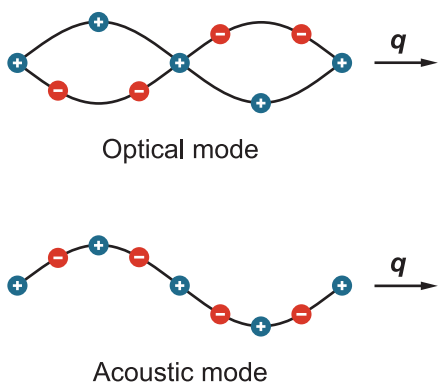

Figure 12: Transverse optical and transverse acoustic waves of a linear chain consisting of two different types of atoms, illustrated by the deflection of the atoms for two oscillations of the same wavelength.

3.2 Polaritons

We will now deal with the optical oscillations in an ionic crystal with a cubic structure. In the ionic crystal, the different atoms in the elementary cell carry different charges. In a cubic structure, the charges compensate each other so that the elementary cell does not show a macroscopic polarization. However, in the case of lattice vibrations, the opposite movement of vicinal atoms with complementary charge generates a strong electric dipole moment (see Figure 12). This causes a strong interaction of the optical phonons with electromagnetic waves. The electric dipole moment also acts on the valence electrons, thus generating a retardation of the propagating wave within the system.

Possible microscopic excitations in a material, which are accompanied by macroscopic electromagnetic fields, are called **polaritons**. These are obtained from self-consistent solutions for the combination of field and constitutive equations adapted to the material.

In the following, we discuss possible excitations for the case of **plane waves**: $\underline{\boldsymbol{E}}(r,t) = \boldsymbol{E}_0 \cdot \exp[i(\boldsymbol{q}\boldsymbol{r} - \omega t)]$, where $\underline{\boldsymbol{E}}$ represents the complex field quantity under study. With this, we obtain the following for the **wave equation** of a non-magnetic dielectric medium without free charges

$$\boldsymbol{q} \times (\boldsymbol{q} \times \boldsymbol{E}) = -\omega^2 \mu_0 (\varepsilon_0 \boldsymbol{E} + \boldsymbol{P}) - i\,\omega\,\mu_0\,\boldsymbol{j} \tag{19}$$

For the further discussion of equation (19), all field vectors are separated into a transverse (T) and a longitudinal (L) component with respect to the propagation direction $\boldsymbol{q}$

$$\boldsymbol{E} = \boldsymbol{E}_T + \boldsymbol{E}_L \quad \text{with} \quad \boldsymbol{q} \cdot \boldsymbol{E}_T = 0 \quad \text{and} \quad \boldsymbol{q} \times \boldsymbol{E}_L = 0 \tag{20}$$

With this separation, we find for the **longitudinal *E*-waves**

$$\omega(\varepsilon_0 \boldsymbol{E}_L + \boldsymbol{P}_L) + i\,\boldsymbol{j}_L = 0 \tag{21}$$

which means that the displacement current and the conduction current have to compensate each other. The longitudinal $\boldsymbol{E}$-wave is therefore not accompanied by a magnetic

field and is *not* able to interact with transverse light waves. In the isotropic case, where the electrical susceptibility $\underline{\chi}_e$ and the conductivity σ are scalar quantities, the complex dielectric function $\underline{\varepsilon}_r$ of the material must have a zero point at the frequency ω_{LO} of the longitudinal $\boldsymbol{E}$-wave

$$\underline{\varepsilon}_r(\omega_{LO}) = 1 + \underline{\chi}_e(\omega_{LO}) + i\frac{\sigma}{\varepsilon_0\,\omega_{LO}} = 0 \tag{22}$$

For every frequency that corresponds to a zero point in $\underline{\varepsilon}_r$, any q-value is allowed.

For **transverse $\boldsymbol{E}$-waves**, we find from equation (19)

$$q^2\boldsymbol{E}_T = \omega^2\mu_0(\varepsilon_0\boldsymbol{E}_T + \boldsymbol{P}_T) + i\omega\mu_0\boldsymbol{j}_T \tag{23}$$

with the complex refractive index $\underline{n}^2 = q^2/q_0^2$ which relates the wave numbers q, q_0 of a wave in matter and in vacuum, respectively, we obtain the *dispersion relation* for transverse $\boldsymbol{E}$-waves for the isotropic case

$$q^2 = \frac{\omega^2}{c_0^2}\underline{n}^2 \quad \text{with} \quad \underline{n} = \sqrt{\underline{\varepsilon}_r} \quad \text{and} \quad c_0 = \frac{1}{\sqrt{\mu_0\,\varepsilon_0}} \tag{24}$$

Here c_0 is the *velocity of light in vacuum*. The dispersion curve of a polariton in a dielectric medium, which is shown in Figure 14, depends on the dielectric properties of the material given by the relation $\boldsymbol{P} = \boldsymbol{P}(\boldsymbol{E})$.

We will now discuss the propagation of an electromagnetic wave in an ionic crystal. This is described by a strong interaction of a *photon* with an optical phonon, called **phonon-polariton** [17]. We must distinguish between the local electric field $\boldsymbol{E}_{loc}$ and the external applied field $\boldsymbol{E}_a$. For a cubic crystal structure, we find from the Clausius-Mossotti equation (Eq. (8))

$$\boldsymbol{E}_{loc} = \boldsymbol{E}_a + \frac{1}{3}\frac{\boldsymbol{P}}{\varepsilon_0} \tag{25}$$

Here, $\boldsymbol{P}$ denotes the total polarization with contributions from both the distorted lattice and the dislocation of the valence electrons, which is proportional to the polarisability of the base molecule α (see Eq. (6)). The contributions are called the **phononic** and the **electronic** polarization, respectively. According to this, the electrical susceptibility $\underline{\chi}_e$ defined by the medium equation (3) can be divided into two parts

$$\underline{\chi}_e = \underline{\chi}_{PH} + \underline{\chi}_{VE} \tag{26}$$

the first one originates from the *lattice vibrations* and the second from the *valence electrons*. For frequencies much lower than the electron resonance, the contribution of the valence electrons has a real and constant value, which is often abbreviated by $\chi_{VE} \equiv \chi_\infty$.

Solving the set of differential equations assuming a *classical damped oscillator* dispersion model for the *phononic* contribution and considering the retardation yields for the total susceptibility

$$\underline{\chi}_e = \frac{\left(-\omega^2 - i\omega\gamma_{TO} + \omega_0^2\right)3N_a\alpha + 3\omega_p^2}{\left(-\omega^2 - i\omega\gamma_{TO} + \omega_0^2\right)\left(3 - N_a\alpha\right) - \omega_p^2} \tag{27}$$

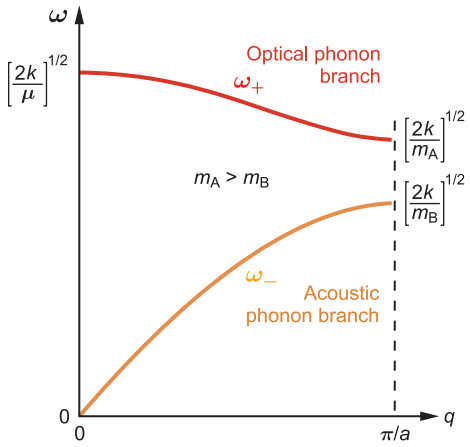

Figure 13: Optical and acoustic phonon branch of the dispersion relation of a linear chain consisting of two different types of atoms.

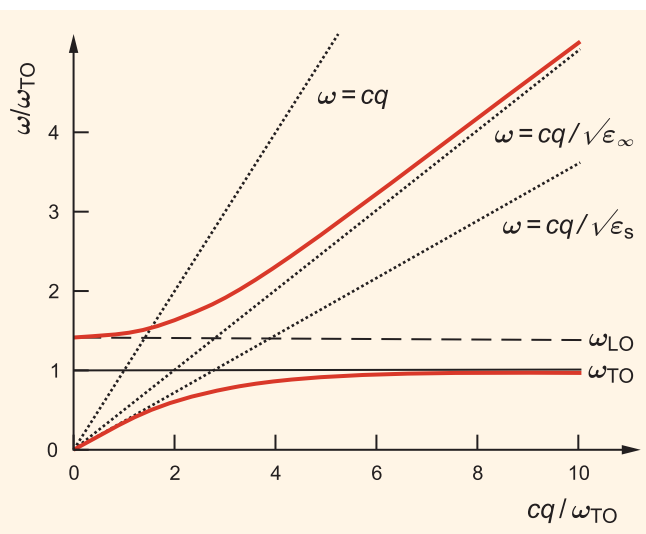

Figure 14: Dispersion curve for a phonon-polariton. The plotted part of the q-values (wave vector) is small in comparison to a reciprocal lattice vector. The lattice dispersion can therefore be neglected.

where γ_{TO} denotes the damping frequency of the transverse optical phonon, ω_0 the resonance frequency of the optical phonon, ω_p the plasma frequency of the ions, N_a the concentration, and α the polarisability.

At the limit of very high frequencies ($\omega \to \infty$), we obtain from Eq. (27)

$$\chi_\infty = \frac{3N_a\,\alpha}{3 - N_a\,\alpha} \tag{28}$$

which is exactly the contribution of the valence electrons to the susceptibility.

It should be noted that the phononic contribution is not only given by the distortion of the lattice but is also influenced by the displacement of the valence electrons, given by $(N_a \cdot \alpha)$.

With the characteristic quantities

$$\omega_p^{*2} \equiv \omega_p^2\left(\frac{\chi_\infty + 3}{3}\right)^2 \quad \text{and} \quad \omega_{TO}^2 \equiv \omega_0^2 - \frac{1}{3}\omega_p^2 \cdot \frac{\chi_\infty + 3}{3} \tag{29}$$

we can rewrite equation (27) in the form of a classical damped oscillator dispersion relation

$$\underline{\chi}_e = \chi_\infty + \frac{\omega_p^{*2}}{\omega_{TO}^2} \cdot \frac{\omega_{TO}^2}{\omega_{TO}^2 - \omega^2 - i\,\omega\,\gamma_{TO}} \tag{30}$$

where $\varepsilon_\infty = 1 + \chi_\infty = n^2$ is the high frequency optical permittivity, which takes into account the contributions of the vibrations of the valence electrons, and ω_{TO} and γ_{TO} denote the eigenfrequency and damping of the transverse optical phonon mode, respectively. The term $(\omega_p^{*2}/\omega_{TO}^2)$ equals the strength of the transverse phonon mode.

Thus, the frequency of the transverse polariton (ω_{TO}) is given by the result of equation (29) and the frequency of the longitudinal polariton (ω_{LO}) is obtained from the zero point of the dielectric function (22). Insertion of $\underline{\chi}_e$ leads to

$$\omega_{LO}^2 = \omega_0^2 + \frac{2}{3}\omega_p^2 \cdot \frac{\chi_\infty + 3}{3\chi_\infty + 3} \tag{31}$$

In the oscillator model, we have taken *damping* into account by the parameter γ. This is predominantly caused by a *decay* of the *polariton mode* in other lattice vibrations due to an *anharmonicity* of lattice forces. The properties of the transverse polaritons are studied by measurements of the reflection and transmission of a sample in the infrared spectral region. The excitation of a sample with an electromagnetic wave generates polaritons in the crystal, which propagate with a defined degree of damping depending on the crystal's properties.

3.3 Consequences of the Concept of Polaritons

For the static limit ($\omega \to 0$), we obtain from equation (30) the static susceptibility $\chi_s \equiv \chi_e'(0)$, and with this the *static limit of the dielectric function*

$$\varepsilon_s \equiv \varepsilon_r'(0) = 1 + \chi_\infty + \frac{\omega_p^{*2}}{\omega_{TO}^2} \tag{32}$$

Insertion of the characteristic quantities (29) and of the resonance frequency of the longitudinal polaritons (31) results in the **Lyddane-Sachs-Teller (LST) relation**

$$\frac{\varepsilon_s}{\varepsilon_\infty} = \frac{\omega_{LO}^2}{\omega_{TO}^2} \tag{33}$$

In 1941, Lyddane, Sachs, and Teller developed this formula for the dependence of the phonon-polariton frequencies and the dielectric properties in the case of ionic polarisation. It defines a correlation between the ratio of the square of the longitudinal (ω_{LO}) and transverse (ω_{TO}) optical mode frequencies at $q = 0$, and the ratio of the values of the real part of the relative dielectric permittivity at frequencies much lower (ε_s) and higher (ε_∞) than the resonance frequency of the ionic relaxation. Again, $\varepsilon_\infty = 1 + \chi_\infty = n^2$ is the high frequency optical permittivity, which takes into account the contributions of the vibrations of the valence electrons.

The LST relation shows that a large value of the permittivity in ionic crystals is connected with a wide gap (stop band) between the eigenfrequencies ω_{LO} and ω_{TO} of the

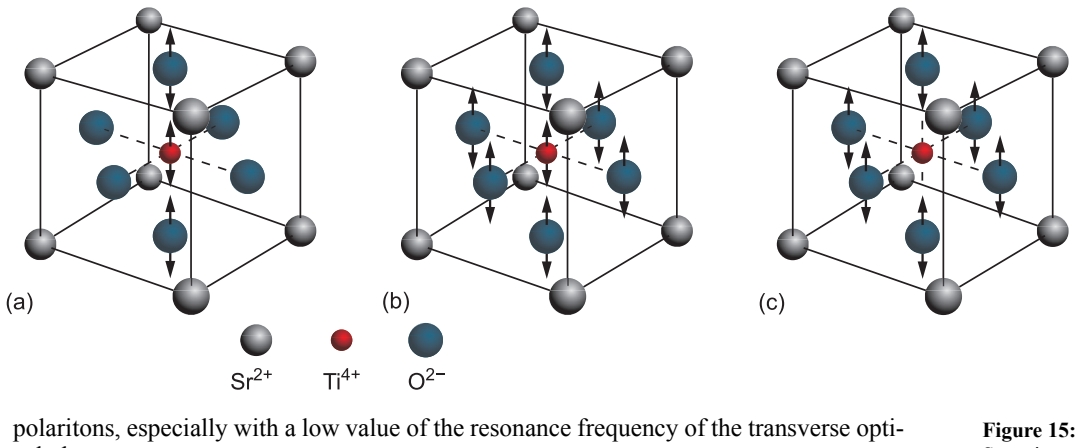

Figure 15: Characteristic oscillations in Strontium titanate:
(a) the linear O^{2-}-Ti^{4+}-O^{2-} chain against the remaining lattice at about 540 cm^{-1};
(b) the Ti^{4+} and O^{2-} ions against the Sr^{2+} sub-lattice at about 180 cm^{-1};
(c) the oxygen octahedron against the sub-lattice constituted by the Sr^{2+} and Ti^{4+} ions. This oscillation takes place at about 87 cm^{-1} and is called the *soft mode*.

polaritons, especially with a low value of the resonance frequency of the transverse optical phonon ω_{TO}.

As a further consequence of the *retardation* ($\boldsymbol{E}_{loc} \neq \boldsymbol{E}_a$) in ionic crystals, it follows that the polarization fields act in different ways on the longitudinal and transverse modes of the vibrating system. Even for the simplest case of rigid ions ($\chi_\infty = 0$), we find from equations (29) and (31) a softening (**mode softening**) of the low frequency *transverse* mode and a *hardening* of the *longitudinal* modes, respectively

$$\omega_{TO}^2 = \omega_0^2 - \frac{1}{3}\omega_p^2 \quad \text{and} \quad \omega_{LO}^2 = \omega_0^2 + \frac{2}{3}\omega_p^2 \tag{34}$$

The low-frequency transverse optical mode is characterized by a partial compensation of short-range lattice forces and long-range electrical fields; the mode becomes *soft*. Under certain temperature and pressure conditions the restoring forces for the transverse optical mode are very weak and a phase transition is induced (see Sec. 4.2).

3.4 Characteristic Oscillations in Perovskite-type Oxides

In the previous sections, we described the lattice vibrations of an ionic crystal with a cubic structure and two atoms per elementary cell. The electric properties of these crystals in the infrared frequency range are derived from the dispersion of the optical phonon modes. We learned that the low-frequency tail of the imaginary part of the susceptibility caused by ionic polarization is responsible for an inherent contribution to the dielectric losses in the frequency range between 1 GHz and 100 GHz, thus the ionic polarization losses limit the quality factor of microwave dielectrics. This is important for the selection of dielectric materials for microwave applications, as explained further in Chap. 36.

In the following, some basic properties of the technically important **alkaline earth titanates** are outlined which can be explained by the model of optical phonons. The alkaline earth titanates exhibit a perovskite crystal structure (see Figure 4). The temperature of the phase transition from the cubic to the distorted or tetragonal structure is approximately 105 K for $SrTiO_3$ and 396 K for $BaTiO_3$, respectively. The latter shows a distortion in the tetragonal lattice cell by a displacement of cations and anions which gives rise to the ferroelectricity of the material (see Sec. 2.5.1).

In this chapter, we consider the dielectric properties of titanates in the high-temperature cubic phase, which permits three different **infrared active modes**. Here, infrared active means that the crystal exhibits a dipole moment induced by the displacement of the ions which can interact with the light wave. The characteristic oscillations of $SrTiO_3$, are depicted as an example in Figure 15. At the highest frequency (540 cm^{-1}), an oscillation of the linear O^{2-}-Ti^{4+}-O^{2-} chain against the remaining sub-lattice occurs (Figure 15a). As a second oscillation (180 cm^{-1}), the O^{2-} octahedron together with the Ti^{4+} ion move against the Sr^{2+} sub-lattice as shown in Figure 15b. At the excitation with the lowest frequency (87 cm^{-1}), that is the **soft mode**, the O^{2-} octahedron oscillates against the Ti^{4+} and Sr^{2+} ions, respectively, so that all negative ions are displaced against all positive ions (Figure 15c).

The frequency dependence of the real and imaginary parts of the complex dielectric function of single crystalline $SrTiO_3$ in the infrared region measured at room temperature is shown in Figure 16. The soft mode at 87 cm^{-1} exhibits the greatest strength of oscillation and the lowest damping compared with the other transverse optical phonons at 180 cm^{-1} and 540 cm^{-1}. The *softening* of the 87 cm^{-1} TO mode describes the fact that the mode's frequency ω_{TO} decreases with decreasing temperature when approaching the

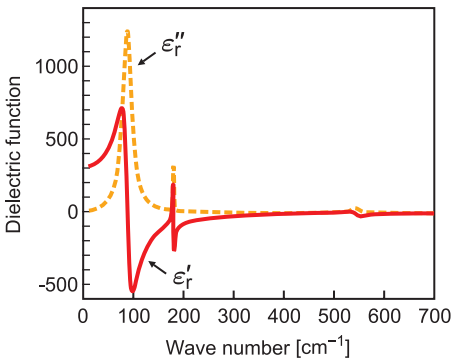

Figure 16: Dielectric function of $SrTiO_3$ in the infrared spectral region with real (outlined) and imaginary part (dotted line).

phase transition temperature coming from high temperatures. For $\omega_{TO} = 0$ the phase becomes unstable due to the vanishing restoring force and a displacive phase transition occurs (see Sec. 4.2).

The temperature dependence of the low-frequency dielectric permittivity $\varepsilon_r'(T)$ of the perovskite-type material in the cubic phase obeys the empirical **Curie-Weiss law**

$$\varepsilon_r'(T) \approx \chi_e'(T) = \frac{C}{T - \Theta} \tag{35}$$

where C is the Curie constant and Θ is the Curie temperature, which in general is equal to or smaller than the temperature T_C of the phase transition: $\Theta \leq T_C$.

According to the Lyddane-Sachs-Teller relation (33), the Curie-Weiss law, that is the increase in the static dielectric constant with decreasing temperature (in the cubic phase), is caused by the decreasing frequency of the transverse optical phonon, which obeys a square root dependence as long as ω_{LO} can be assumed to be independent of the temperature

$$\omega_{TO} \propto \sqrt{T - \Theta} \quad \leftrightarrow \quad \omega_{TO}^2 \propto (T - \Theta) \tag{36}$$

The correlation between the temperature dependencies of the relative permittivity (Eq. (35)) and the frequency of the soft-phonon mode (Eq. (36)) has been confirmed for $SrTiO_3$, as will be shown in Sec. 4.2.

In Sec. 3.1, we discussed an idealized ionic lattice built from harmonic oscillators. A harmonic potential means that the restoring force is a linear function of the displacement. In the case of a real ionic lattice, the local field generated by the neighboring atoms leads to an *anharmonic potential* for each ion, and thus to a non-linear restoring force. The consequence of this is that the linear dependence between the dielectric displacement $\boldsymbol{D}$ and the electric field $\boldsymbol{E}$ (see Eq. (4)) no longer holds. Instead, we have to introduce a *field-dependent* permittivity $\underline{\varepsilon}_r(E)$. The effect of this non-linearity becomes significant at high electric fields. Hence, the effect is more frequently observed in thin films than in bulk dielectrics because high electric fields are more easily reached at moderate voltages. In addition, for a given electric field the effect is more pronounced for higher permittivities. A high permittivity corresponds to a smaller restoring force between the ions of the lattice and a large atomic displacement at a given field. An example of field-dependent permittivity is shown in Figure 17. The non-linear electrical permittivity $\underline{\varepsilon}_r(E)$ is exploited for voltage tunable microwave devices (see Chap. 36).

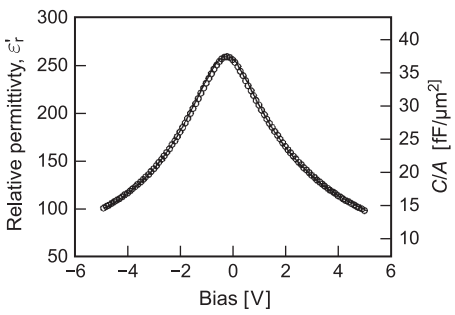

Figure 17: Non-linearity of permittivity of a $(Ba_{0.7}Sr_{0.3})TiO_3$ thin film prepared by MOCVD [25].

4 Ferroelectrics

Having introduced the concept of polaritons to describe the properties of materials in the dielectric state, we will now turn our attention to dielectric crystals in the ferroelectric state, where the material exhibits a spontaneous electric polarization and in which the direction of the polarization can be reoriented between crystallographically defined states by an external electric field. Phase transitions will be described in terms of a mean-field or Ginzburg-Landau theory as a consequence of the long-range Coulomb interaction. In the microscopic description by phonon-polaritons, the displacive phase transition will be understood as a polarization catastrophe. The properties of some prominent ferroelectric materials will be given as examples. Finally, we will deal with typical static domain configurations, the motion of domain walls and the basics of ferroelectric switching.

4.1 Ginzburg-Landau Theory

In this Section, we describe the **thermodynamics** of the ferroelectric phase transitions in terms of a **Ginzburg–Landau theory**. This theory is equivalent to a **mean field theory**, where the thermodynamic entity is considered in the mean field of all the others. Such a theory is a good approximation if the dipole interacts with many other dipoles. As a consequence of the long-range Coulomb interaction, this condition is generally fulfilled for the ferroelectric phase transitions.

The Ginzburg–Landau theory introduces an **order parameter** P – here the polarization – which for a second-order phase transition diminishes continuously to zero at the phase transition temperature T_C. Close to the phase transition, therefore, the **free energy** may be written as a function of powers of the order parameter

$$\mathfrak{F}(P,T) = \int dV \left[\frac{1}{2} g_2 P^2 + \frac{1}{4} g_4 P^4 + \frac{1}{6} g_6 P^6 + \frac{1}{2} \delta (\nabla P)^2 - \frac{1}{2} PE \right] \tag{37}$$

In this expansion, the odd powers of P do not occur because of symmetry reasons. We shall see that by including powers up to the sixth order, we will also be able to describe first-order phase transitions. The gradient term $(\nabla P)^2$ in Eq. (37) penalizes spatial inhomogeneities. It will become important when we consider ferroelectric domains. At present, we will neglect this term and replace the functional of Eq. (37) with a polynomial representing the free energy density

$$F(P,T) = \frac{1}{2} g_2 P^2 + \frac{1}{4} g_4 P^4 + \frac{1}{6} g_6 P^6 - \frac{1}{2} PE \tag{38}$$

The coefficient g_6 needs to be larger than zero because otherwise the free energy would approach minus infinity for large P. All coefficients depend on the temperature and in particular the coefficient g_2 may be approximated by

$$g_2 = C^{-1} (T - \Theta) \tag{39}$$

Eq. (39) is a result of a temperature expansion around Θ whereas the **Curie temperature** Θ is equal to or less than the **phase transition temperature** T_C. The Ginzburg–Landau theory leads to power law expressions for the thermodynamic quantities close to the phase transition. The so-called **critical exponents** are characteristics of phase transitions in general. Depending on the universality class of the statistical mechanical ensemble, they assume values independent of the particular system.

In the following, we will consider the thermodynamic states with the conjugated field $E = 0$. Stable states are characterized by minima of the free energy density

$$\begin{aligned} \frac{\partial F}{\partial P} &= 0 \quad = \quad P\left(g_2 + g_4 P^2 + g_6 P^4\right) \\ \frac{\partial^2 F}{\partial P^2} &= \chi_e^{-1} \; = \; g_2 + 3 g_4 P^2 + 5 g_6 P^4 > 0 \end{aligned} \tag{40}$$

Eqs. (40) are the necessary and sufficient conditions for a minimum of F. They are solved by $P = 0$, the condition of the **paraelectric** phase. Further solutions exist for $P_s > 0$; these are the **ferroelectric** phases.

4.1.1 Paraelectric Phase

In this case we have $P = 0$. Inserting Eq. (39) into Eq. (40), we immediately see that above T_C the coefficient g_2 needs to be larger than zero in order to obtain stable solutions. A comparison of Eqs. (39) and (40) shows that g_2 is expressed by the susceptibility χ_e, for which a **Curie-Weiss law** is found

$$\chi_e(T) = \frac{C}{T - \Theta} \propto (T - \Theta)^{-\gamma} \; ; \; \gamma = 1 \tag{41}$$

In the language of the critical exponents close to T_C, the susceptibility follows a power law in $(T - \Theta)$. For the critical exponent γ, the Ginzburg-Landau theory gives $\gamma = 1$. In this derivation, it is assumed that the temperature dependencies of g_4 and g_6 are comparatively small close to T_C.

4.1.2 Ferroelectric Phases – Second-Order Phase Transition

We will now consider the second-order phase transition to the ferroelectric state (compare Sec. 2.5.1 and Figure 5). In this case, we have to take $g_4 > 0$ and neglect the coefficient g_6. It follows that

$$\frac{\partial F}{\partial P} = P\left(C^{-1}(T - \Theta) + g_4 P^2\right) \tag{42}$$

with the solutions

$$P = 0 \quad \text{or} \quad P_s^2 = -\frac{(T - \Theta)}{g_4 C} \tag{43}$$

For $T < \Theta$, a spontaneous polarization exists. The Curie temperature Θ is equal to the phase transition temperature T_C

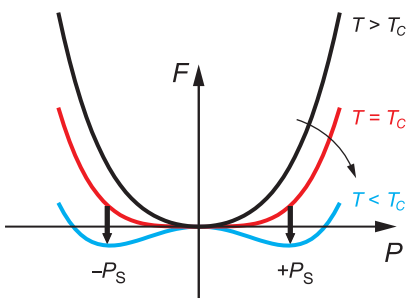

Figure 18: Free energy density as a function of the polarization for a ferroelectric with a second-order phase transition as a function of temperature. Below T_C, the minimum of the free energies continuously shifts towards finite values of P_s.

$$P_s = \left(\frac{1}{C\,g_4}\right)^{1/2} (T_C - T)^{1/2} \propto (T_C - T)^{\beta} \tag{44}$$

The order parameter, namely the spontaneous polarization, depends with a square root law on the distance from the phase transition. In the language of the **critical exponents**, the Ginzburg-Landau theory predicts a power law for the order parameter. The critical exponent β takes the value ½.

Figure 18 schematically displays the free energy density close to the second-order phase transition for different temperatures as a function of the order parameter P. For $T > T_C$, a minimum is found for $P = 0$. At $T \leq T_C$, this minimum shifts continuously to final values of the polarization.

Inserting Eq. (44) into Eq. (40), we obtain the temperature dependence of the susceptibility below the phase transition temperature

$$\chi_e^{-1}\big|_{T<T_C} = 2\,\frac{(T_C - T)}{C} \tag{45}$$

Comparing Eq. (45) with Eq. (41) reveals that the susceptibility prefactor changes at a phase transition by a factor of two. It is important to note here that the susceptibilities calculated in this manner are isothermal susceptibilities [18], while typical measurements of the susceptibility using a capacitance bridge under small alternating currents are adiabatic measurements. As a result, the predicted ratio in slopes is not always observed experimentally.

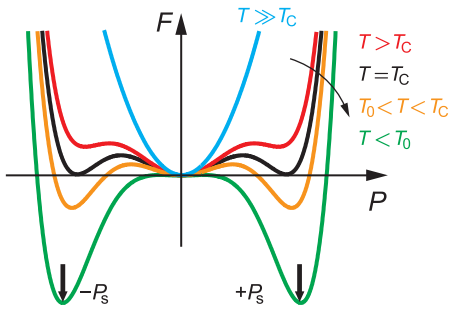

Figure 19: Free energy density as a function of polarization for a ferroelectric with a first-order phase transition as a function of temperature.

4.1.3 Ferroelectric Phases – First-Order Transition

We will now discuss first-order transitions in ferroelectric systems. For this purpose in the free energy equation (Eq. (37)), we have to choose $g_4 < 0$ and $g_6 > 0$. The stable states are once again defined by Eq. (40) with solutions $P = 0$ or

$$P_s^2 = \left(|g_4| + \sqrt{g_4^2 - 4C^{-1}\,(T - \Theta)\,g_6}\right) \Big/ 2g_6 \tag{46}$$

The positive sign and the bracket are required in order to obtain a stable solution. We will now consider the temperature behavior of the free energy density at the value of the spontaneous polarization:

1) for $P = 0$ we have $F = 0$.
2) for P_s from Eq. (46), we obtain the following after insertion into Eq. (37)

$$F(P_s,T) = \frac{1}{24\,g_6^2}\left(|g_4|\left(6g_2g_6 - g_4^2\right) - \left(g_4^2 - 4g_2g_6\right)^{3/2}\right) \tag{47}$$

The free energy density becomes zero for

$$g_2 = \frac{3g_4^2}{16\,g_6} = \frac{(T_C - \Theta)}{C} \tag{48}$$

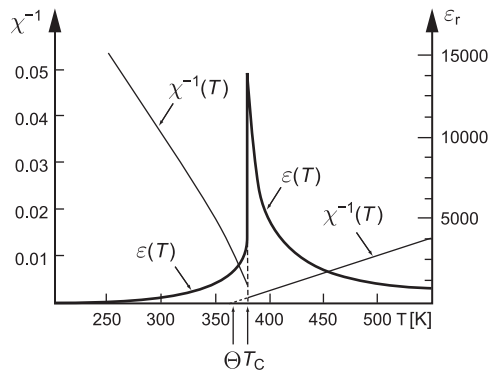

Figure 20: Schematic presentation of the prediction from the Ginzburg-Landau theory for the reciprocal susceptibility or the dielectric constant of a system with a first-order phase transition.

Figure 19 schematically displays the free energy density as a function of polarization for some relevant temperatures. Above a temperature T_C, the free energy assumes a parabolic shape with a minimum corresponding to a stable paraelectric phase. During cooling, secondary minima at finite polarizations become visible. Their energy level at the beginning, however, is higher than that at $P = 0$. In this regime, the paraelectric phase is stable and the ferroelectric phase meta-stable. Lowering the temperature further, at $T = T_C$ we reach the situation where all three minima of the free energy are at the same level. For the temperatures below T_C, F becomes negative and favours a finite spontaneous polarization. In the temperature regime between T_C and Θ, the paraelectric phase coexists with the ferroelectric phase with the paraelectric phase being meta-stable. Somewhere during cooling through this regime, the first-order phase transition to the ferroelectric state will occur with a corresponding jump in the spontaneous polarization from zero to a finite value.

We will now consider the susceptibility. Following Eq. (40) for $T > T_C$, a Curie-Weiss law is again found with an apparent critical temperature Θ that does not coincide with the first-order phase transition temperature T_C. The ratio of the susceptibilities below and above T_C now takes a value of four. Figure 20 schematically displays the susceptibilities calculated in terms of the Ginzburg–Landau theory close to the phase transition. A comparison of the susceptibilities for barium titanate (see Figure 5) reveals good qualitative agreement.

4.2 Soft Mode Approach of Displacive Phase Transition

The existence of the local electric field in ionic crystals leads to a splitting of the optical vibration modes (see Sec. 3.2). It was shown that the polarization fields act in different ways on the longitudinal and transverse modes of the vibrating system. The *longitudinal mode* frequency is shifted to higher frequencies while the *transverse mode* is softened (see Eq. (34)). If we look at the zone centre, we realize the large splitting of the longitudinal and transverse optic modes. In the case of the longitudinal optical mode, the polarization field enhances the mechanical restoring force. The *mode softening* of the transverse modes originates from a partial compensation of the short-range lattice (elastic) forces on the one hand and the long-range electric fields on the other hand. This effect is strongest at the zone centre. We will now look at the consequences of this for the transition into the *ferroelectric phase*.

If the compensation effect between the elastic and the electric forces is complete, then the transverse optic mode frequency, Eq. (34) becomes zero, caused by a decrease of temperature,

$$\omega_{TO}^2 \equiv \omega_0^2 - \frac{1}{3}\omega_p^2 \cdot \frac{\chi_\infty + 3}{3} \quad \rightarrow \quad 0 \tag{49}$$

and the **soft phonon** condenses out so that a phase transition to a state with spontaneous polarization takes place. In the case of the softening of the TO mode, the transverse frequency becomes zero and no vibration exists anymore (“frozen in”).

This **soft-mode phase transition** can be studied by neutron scattering, where the phonon dispersion can be studied as a function of reciprocal lattice vector q. Figure 21 displays results for the **phonon dispersion** of the transverse modes in $SrTiO_3$ for different temperatures and along two directions [27]. For small reciprocal lattice vectors q, the transverse optical phonon softens significantly at the zone centre. Furthermore, such a softening is also observed for the transverse acoustic mode at the zone boundary in (111) direction.

Figure 22 displays $(\omega_{TO})^2$ at the zone centre as a function of temperature for strontium titanate. A linear relation is found, suggesting that the temperature dependence of the optical mode frequency relates to the phase transition. In accordance with the *Lyddane–Sachs–Teller relation* (see Sec. 3.3), $(\omega_{TO})^2$ relates directly to the dielectric constant. From the extrapolation according to Eq. (41), a phase transition close to $\Theta = 50$ K would be expected. This phase transition, however, does not really take place in $SrTiO_3$. It is dominated by a competing displacive phase transition at the zone boundary. The softening of the acoustic zone boundary phonon can be read off from the dispersion relations in the (111) direction.

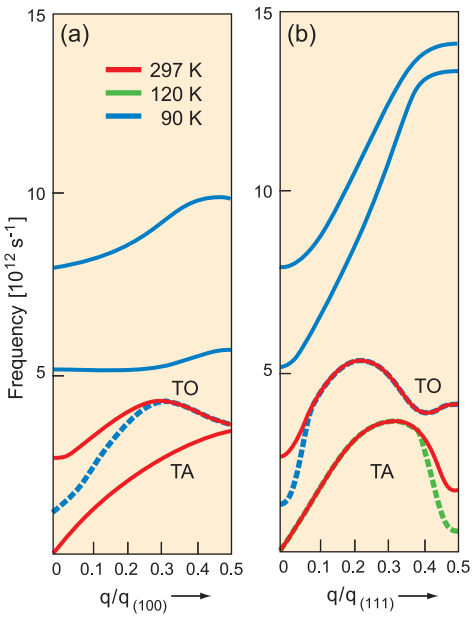

Figure 21: Phonon dispersion relations for the transverse modes for strontium titanate.
(a) (100) direction
(b) (111) direction. Phonons soften not only at the zone center but also at the zone boundary for the (111) direction.

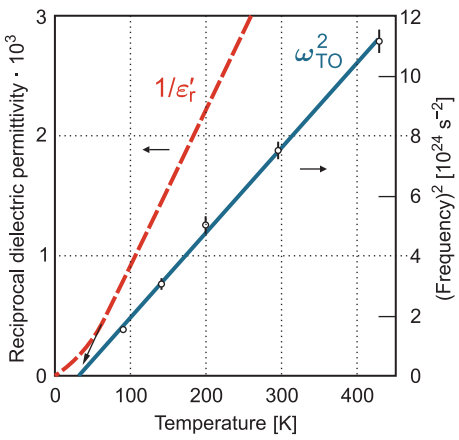

Figure 22: Square of the frequency of the transverse optic zone centre mode for $SrTiO_3$ as a function of temperature (solid line) derived from neutron scattering experiments [3]. The dashed line shows the Curie-Weiss behavior of the reciprocal of the relative permittivity.

4.3 Ferroelectric Materials

A comprehensive list of ferroelectric crystals is given in the Landolt and Börnstein monographs [27], [28]. Among the class of **ionic crystals**, **perovskites** are the commercial most important group. Ferroelectric materials are widely used in applications such as capacitors (e.g. $BaTiO_3$, where the high dielectric constant is utilized), electromechanical transducers (e.g. $Pb(Zr_{1-x}Ti_x)O_3$, which is attractive because of its high piezoelectric coefficients), pyroelectrics (e.g. modified $PbTiO_3$, $(Sr, Ba)Nb_2O_6$), electro-optic components (e.g. $LiNbO_3$), and in non-volatile ferroelectric capacitors for memory applications (e.g. $Pb(Zr_{1-x}Ti_x)O_3$).

One of the most important ferroelectric and piezoelectric materials is the $PbZrO_3$-$PbTiO_3$ (**PZT**) solid solution. Over the entire solid solution range, PZT adopts distorted versions of the perovskite structure, as shown in Figure 23. At the so-called **morphotropic phase boundary** (MPB), the tetragonal phase and the rhombohedral phase are both observed. This leads to the presence of 14 polarization directions (6 along the <001> family from tetragonal phase, and 8 along <111> for the rhombohedral polytype) which are equivalent, or nearly equivalent, in free energy. The result is that the morphotropic phase boundary corresponds to a highly polarizable state. Thus, it is reasonable that the dielectric and piezoelectric properties show strong maxima near this composition. Recently, it has been suggested that at low temperatures, a monoclinic phase is stabilized near the MPB [29]. It is unknown whether such a phase also contributes to the enhanced polarisability near the MPB. Whatever the source, the high *piezoelectric coefficients* (i.e. d_{33} values of $\sim$ 250 to 400 pC/N, depending on the doping), coupled with a high transition temperature are the main reasons that PZT ceramics are so widely used as piezoelectric sensors and actuators.

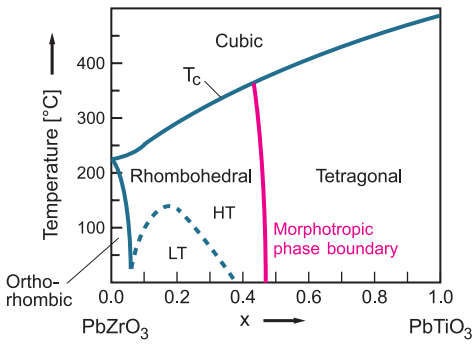

Figure 23: Phase diagram for PZT showing the morphotropic phase boundary between rhombohedral and tetragonal phases after [23].

It is important to realize that **thin films** may differ in substantially from bulk ceramics or single crystals of the same composition. One of these differences is the substantial in-plane stresses that thin films are typically under, ranging from MPa to GPa [30]. As many ferroelectric materials are also ferroelastic, imposed stresses can markedly affect the stability of the ferroelectric phase, as well as the ease with which polarization can be reoriented in some directions. Figure 24 shows an example of this, where the *phase diagram* for tetragonal $BaTiO_3$ is re-calculated for the case of a thin film without misfit dislocations [31], [32]. It is clear that the phase diagram is considerably complicated by the presence of a dissimilar substrate.

4.4 Ferroelectric Domains

Ferroelectric materials form domain structures. A **domain** is a region with a uniform direction of spontaneous polarization. In the case of tetragonal $BaTiO_3$, when the material undergoes ferroelectric transition, the Ti^{4+} ion displaces towards one of the neighboring oxygen ions. Due to the fact that the Ti^{4+} is octahedrally coordinated, there are six possible directions in which Ti^{4+} can move. Consequently, there are six possible *domain states* for tetragonal $BaTiO_3$. Similarly, in other systems, the permissible **domain states** are governed by the crystallography of the system and by the symmetry elements lost on transforming from the prototype state.

The boundaries between domains are referred to as **domain walls**. Domain walls in ferroelectrics are typically quite thin ($\sim$ 1–10 lattice parameters across) and can therefore be regarded as abrupt changes in the polarization direction. Domain walls are characterized by the angle between the polarization directions on either side of the wall. Thus a 180° domain wall demarks a boundary between anti-parallel domains, while a 90° wall in tetragonal $BaTiO_3$ would be formed at the boundary between domains pointed "up" and "left", for example. The allowed angles for domain walls depend on the orientations of the spontaneous polarization allowed by symmetry. Thus, in rhombohedrally distorted perovskites, there are no 90° domain walls, but instead 71° and 109° walls. A more complete picture of the way the polarization changes as a domain wall is crossed is given by Cao and Cross [33].

Domain walls typically appear along specific crystallographic planes that correspond to conditions of mechanical compatibility [34]. For example, in tetragonal $BaTiO_3$, the {101} family of domain walls corresponds to cutting the unit cell along a face diagonal, and then reassembling the crystal after rotating one piece $\sim$ 90°. A second constraint on the angles between domains corresponds to the fact that in a highly insulating material, it is not energetically favorable to arrange domains in a head-to-head configuration [33]. Such a configuration can be stabilized, however, by the accumulation of a compensating charge at such a domain wall.

For a fully compensated *ferroelectric single crystal* (i.e. one that has picked up sufficient surface charges from electrodes or some other source to compensate the polarization) of a suitable orientation, a **single-domain state** is the lowest free energy. However, in most other cases, domain formation will be driven by either the electrical or mechani-

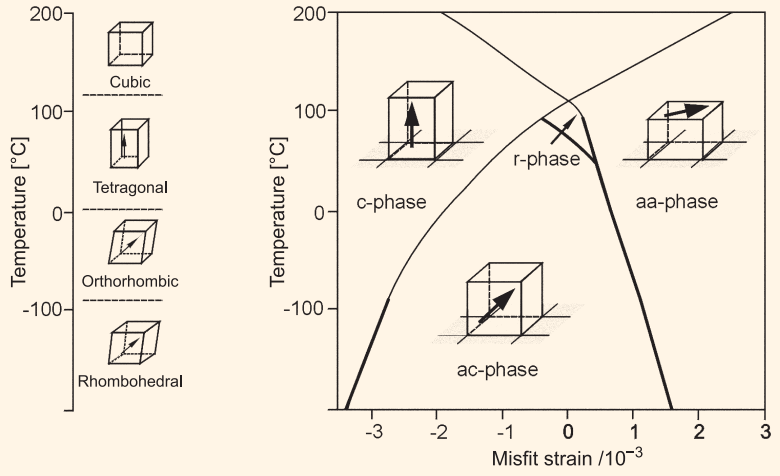

Figure 24: Phase diagram for a (001) $BaTiO_3$ epitaxial film as a function of misfit strain [31]. The notations refer to the polarization direction preferred by a single domain film. The *r* phase has components of the polarization in all three directions.

cal boundary conditions. For instance, at the surface of an uncompensated ferroelectric, the divergence of the polarization results in the appearance of a **depolarizing electric field** [20]. The energy associated with this can electrically drive domain formation (see Figure 25). Similarly, in ferroelectrics which are ferroelastic as well, mechanical stresses can also affect the equilibrium domain formation. It should be noted, however, that it is energetically costly to put a domain wall into a system, since the domain wall, like any other surface, has an associated surface free energy. As a result, the material will not continue to subdivide into smaller and smaller domains. Instead, a balance is reached between the energy required to create the wall and the energy gain from the reduction in total energy. This energy balance will also depend on the grain size of the system [35], so the equilibrium domain size typically drops as the grain size is reduced.

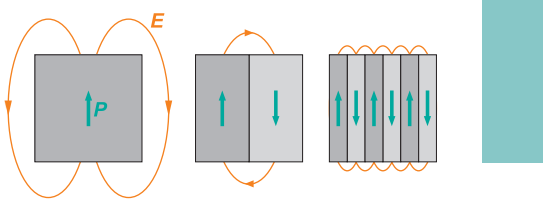

Figure 25: Domain formation driven by reducing the electrical depolarisation energy.

4.4.1 Static Domain Configurations

It is interesting to consider first how domain configurations are determined in **bulk ferroelectrics**, and then to see how these are modulated in thin films.

In general, domain structures in equilibrium are formed to minimize the total energy in the crystal [36], including electric and mechanical strain fields

$$W_{\text{tot}} = W_{\text{M}} + W_{\text{E}} + W_{\text{DW}} + W_{\text{S}} = \min \tag{50}$$

where W_{M} denotes the *elastic*, W_{E} the *electric*, W_{DW} the *domain wall* and W_{S} the *surface energy*.

Thus, the equilibrium domain structure of a ferroelectric should depend on both the electrical and mechanical boundary conditions imposed. For uncompensated domains, electrostatic considerations can drive the formation of anti-parallel domains in many ferroelectrics. It is also important to recall that ferroelectric materials typically develop a spontaneous strain (deformation) as a result of the appearance of spontaneous polarisation. For example, each barium titanate unit cell deforms from a cubic to a tetragonal shape on cooling below the Curie temperature. Figure 26 displays the tetragonal distortion of the barium titanate crystal at the transition.

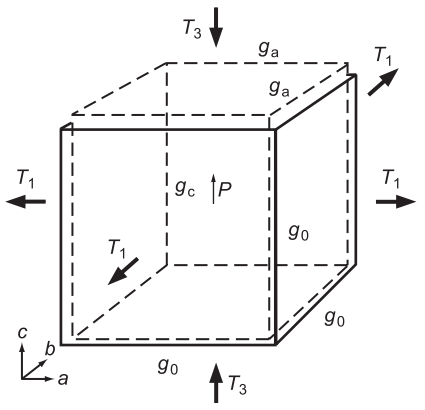

Figure 26: Spontaneous tetragonal deformation of a cubic grain. The cube edges correspond to the crystallographic axis.

If the material is completely clamped, then compressive stresses T_3 and tensile stresses T_1 would be necessary in order to keep the material in its original shape. These clamping stresses may be calculated on the basis of the strain tensor $\boldsymbol{S}_0$, describing the tetragonal distortion. The clamping stresses follow from **Hooke's law**

$$T_i = \sum c_{ij}\, S_j \tag{51}$$

where c_{ij} are the elastic constants.

The stresses have to be chosen so that they minimize the elastic energy. With the elastic constants and the tetragonal distortions for $BaTiO_3$, $W_{\text{M}} = 2.08 \cdot 10^6\ \text{J/m}^3$ evolves. For the tensile and compressive stresses, we find $T_1 = 190\, f_{11}$ MPa and $T_3 = -380\, f_{31}$ MPa, respectively, where the coefficients f_{11} and f_{31} account for possible elastic depolarisation effects.

Another possible way of reshaping the tetragonally distorted cube is a shear in the (110) direction combined with a longitudinal deformation in the (100) direction. In general, a grain can reduce its energy by **twinning**, as shown in Figure 27.

Given the electrical and mechanical driving forces for forming domains, it is clear that there is an overall reduction in the free energy of many ferroelectric samples as domain formation proceeds. However, there is also an energy cost associated with forming the domain wall. Thus, the system will typically drive to an equilibrium domain width. It can be shown that the thickness of the twin should be proportional to the square root of the size of the grain. The situation becomes even more complicated for a *polycrystalline ensemble*. Here, each region of the material is not free to deform, but is constrained by the material around it. Any deformation will cause high internal stresses. To minimize this, complicated domain patterns form.

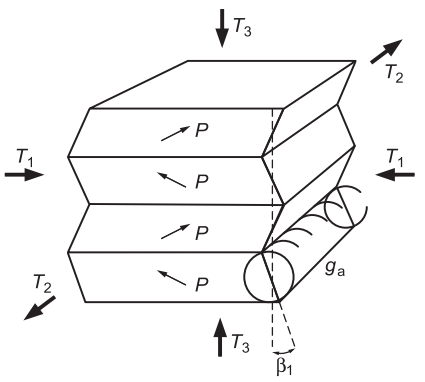

Figure 27: The spontaneous deformation is reduced by twinning. Serration appears at the grain boundary. Homogeneous stresses *T* as indicated can restore the gross cubic shape.

As the equilibrium domain configuration depends explicitly on the mechanical and electrical boundary conditions for the ferroelectric, it is not surprising that domain configurations (and even the thermodynamic stability of the ferroelectric phase) can change as we move from a bulk to a **thin film** sample [37], [38]. A good example of this is given in the work of Pertsev et al. where revised phase diagrams for $BaTiO_3$ and $PbTiO_3$ epitaxial films were derived (see Figure 24) as a function of the *misfit strain* between the substrate and the film [31]. Among the consequences were changes in the order of the phase transition (from 1st to 2nd order), stabilization of the rhombohedral phase to unusually high temperatures, and constraints on the allowed domains. Many of these same ideas are also observed in polycrystalline films.

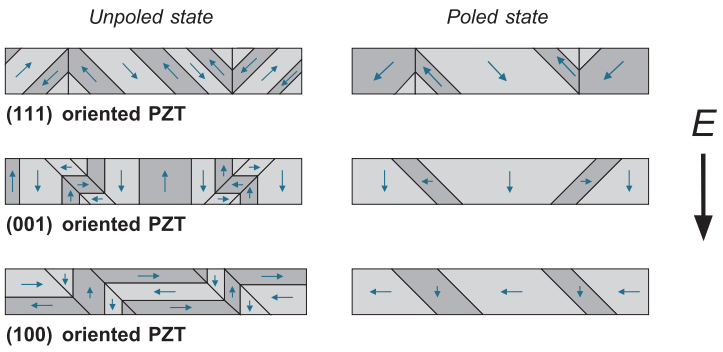

Figure 28: Domain structures of tetragonal PZT with different orientations (see text).

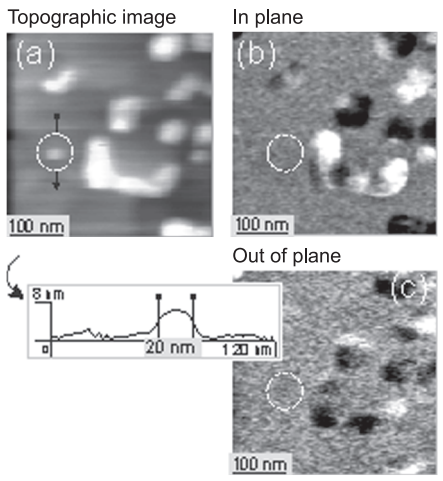

Figure 29: The topographic image
(a) shows eleven PTO grains of sizes from 100 nm down to 20 nm indicated by the circles. In the line scan over the grain denoted by an arrow, shown at the bottom, the size of the grains can be determined.
In the PFM images, the
(b) in-plane and
(c) out-of-plane piezoresponse of the 20 nm grain is not visible, leading to the assumption that these grains do not have any permanent polarization [44].

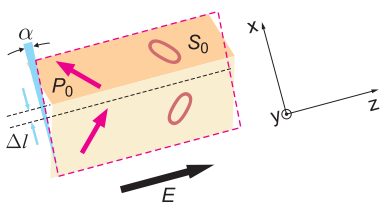

Figure 30: Shift of a 90° domain wall Δl changes the electrical and the elastic dipole moments causing a shear of the domain twin.

Thus, PZT and $BaTiO_3$ films, which are under considerable *tensile stress* on cooling through the phase transition temperature, typically have the polarization tilted substantially into the film plane, while films under compressive stress show large out-of-plane polarizations [39]. In Figure 28, possible domain patterns of different textures of tetragonal films of $PbZr_{0.52}Ti_{0.48}O_3$ are depicted. In the case of *compressive stress*, predominantly (001) orientation, 90° as well as 180° domains are expected [40]. Under the influence of an electric field, the number of 180° domains is decreased. The resulting pattern predominantly consists of 90° domains. In the case of *tensile stress*, predominatly (100) orientation, the change of the domain structure by poling is similar to the (001) orientation, but the a-axis orientation is still preferred [41]. In standard systems for ferroelectric thin films, the orientation of the crystallographic axes of PZT is in the (111) direction. Tuttle et al. have shown that for many thin films the ferroelastic domain structure developed on cooling from the prototype phase is largely retained at lower temperatures, so that switching on non-180° domains is limited [42].

The three-dimensional **piezoresponse force microscope** (PFM) enables the visualization of the domains in thin films and their polarization directions. In epitaxial PZT thin films grown on a (001) single crystalline $SrTiO_3$ substrate coated with $La_{0.5}Sr_{0.5}CoO_3$ oxide layer, a **self-polarization** mechanism was found. Detailed investigations show that the out-of-plane polarization in *c* domains points preferentially towards the bottom electrode and a resulting remanent polarization exists without applying an external field [43]. The domain configuration is always of the "head-to-tail" type.

The influence of **clamping in thin ferroelectric films** becomes clear when dense films are compared with single separated grains. Applying the PFM technique to lead titanate (PTO) films, it was found that the PTO grains in dense films contain laminar 90° domain walls, whereas separated PTO grains show more complicated structures of mainly 180° domain walls. For grains smaller than 20 nm, no piezoresponse signal was observed (Figure 29). When the thickness of a dense epitaxial thin film is reduced, the piezoelectric activity is observed down to 4 nm [45]. The one-dimensional shrinking (as in dense films) leads to different stresses and to varying stabilities of the ferroelectric phase compared with the three-dimensional phase (as in single grains).

4.4.2 Reversible and Irreversible Polarization Contributions

Under sufficiently small electric fields, all dielectrics follow a linear relation, described by $\boldsymbol{D} = \varepsilon \boldsymbol{E}$. This dielectric **small signal response** is caused by reversible contributions of the electronic and ionic polarization processes (intrinsic), as shown in Sec. 2.3. In ferroelectric polycrystalline materials, additional extrinsic mechanisms exist due to the **movement of domain walls** and the alignment of defects

$$\varepsilon_{\text{tot}} = \varepsilon_{\text{intrinsic}} + \varepsilon_{\text{extrinsic}} \tag{52}$$

It has been shown that especially the electromechanically active, non-180° domain walls – that is 90° domain walls in tetragonal structures, 71° and 109° domain walls in rhombohedral structures and so on – are responsible for a considerable contribution to the *dielectric coefficient* as well as to the piezoelectric and the elastic coefficients. The shift of the wall is clearly displayed in Figure 30, whereby favorably oriented domains with respect to the applied field grow at the expense of unfavorably oriented domains. This leads to a change in the electric and the elastic dipole moment ($\Delta \boldsymbol{p}$ and $\Delta \boldsymbol{v}$) and, therefore, to contributions to the dielectric and piezoelectric response. A separation of the intrinsic polarization process from that of the non-180° domain wall is possible by dielectric high frequency measurements in the GHz range. There, these kinds of domain walls do not contribute to ε_{tot}. The mechanism is caused by the fact that a vibrating non-180° wall acts as an emitter of **elastic shear waves** (see Figure 30) propagating at the shear wave velocity c_{Sh} through the crystallite. When the frequency of the applied electric field

corresponds to c_{Sh}, the vibration of the domain wall is suppressed and a strong dielectric relaxation is observed. In ferroelectric thin films, the relaxation step is not found. This is further evidence that non-180° domain wall processes in ferroelectric thin films are strongly limited. However, ferroelastic non-180° domain walls can move when the clamping effect is significantly reduced by patterning the film into discrete islands [46].

When the electric field is increased, the dielectric behavior of ferroelectric material changes from linear to non-linear and hysteretic. The ferroelectric hysteresis is caused by the existence of **irreversible polarization processes** as explained by the Ginzburg–Landau theory (see Sec. 4.1). However, the exact interplay between the polarization reversal of a ferroelectric lattice cell, domain walls, defects and the overall appearance of the ferroelectric hysteresis is still not precisely known. In addition, the above-mentioned reversible processes in ferroelectrics have to be taken into account. The separation of the total polarization into reversible and irreversible contributions that has long been appreciated in the study of ferromagnetic materials [47] might facilitate the understanding of ferroelectric polarization mechanisms.

Two major mechanisms could cause *irreversible processes*: first, **lattice defects** that interact with a domain wall and prevent it from returning into its initial position after removing the electric field that initiated the domain wall motion ("pinning") [48]; second, nucleation and growth of **new domains** which do not disappear after the field is removed again. In ferroelectric materials, the matter is further complicated by defect dipoles and free charges that not only contribute to the measured polarization but can also interact with domain walls [49].

The motion of a domain wall under an external electric field takes place in a statistical potential generated by their interaction with the lattice, point defects, dislocations, and neighboring walls. *Reversible movement* of the wall is regarded as a small displacement around a local minimum. When the driving field is high enough, irreversible jumps above a potential barrier into a neighboring local minimum occur (see Figure 31). Based on these assumptions the measurement of the large signal ferroelectric hysteresis with additional measurements of the small signal capacitance at different bias voltages are interpreted in terms of reversible and irreversible parts of the polarization. As shown in Figure 32, the separation is done by subtracting the reversible part from the total polarization, that is the integrated $C(V)$ curve [50]

$$P_{\mathrm{irr}}(V) = P_{\mathrm{tot}}(V) - \frac{1}{A}\int_0^V C(V')dV' \tag{53}$$

Typical hysteresis loops are dynamically recorded at certain frequencies. If slow reversible polarization mechanisms also contribute to the total polarization P_{tot}, the shape of the hysteresis loop, especially the coercive field, becomes frequency-dependent. To overcome this influence, measurements should be performed with the lowest frequency possible, that is quasi-statically [51].

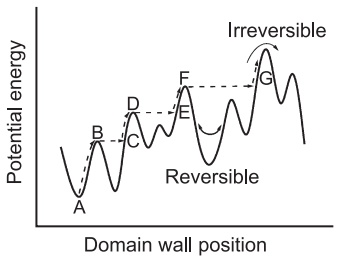

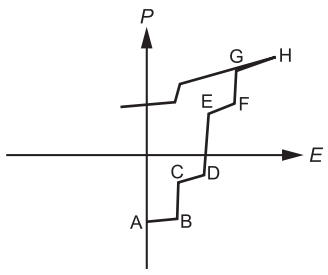

Figure 31: Motion of a domain wall in the statistical potential (top) and correlated hysteresis loop (bottom).

4.4.3 Switching for Ferroelectric Domains

Since many applications of ferroelectric materials require either that the material be poled once, as in a piezoelectric device, or that it be switched repeatedly, as in a memory, it is interesting to consider how domain reversal occurs. As described by Merz [52], **switching** takes place by processes of **domain nucleation** and **domain wall motion**. Apparent sideways motion of domain walls typically occurs by nucleating a step on the domain wall. This protrusion then rapidly grows along the length of the wall, effectively increasing the size of the more favorably oriented domain.

One way to monitor the **switching process** is to measure the current flow through the ferroelectric as a function of time. When an electric field of the same polarity is applied to a fully poled single crystal, there is an initial current flow that corresponds to charging the capacitor. If an opposite polarity field is now applied, in addition to the charging current, additional current flows as a consequence of domain reorientation. Subtracting these two signals enables the current flow associated with the switching process itself to be isolated.

Under conditions where the electric field is constant during the reversal process, then the maximum displacement current, I_{max}, and the switching time, t_s, are given by

$$I_{\max}(E) = I_0 \exp\left(-\frac{\xi}{E}\right) \quad \text{and} \quad t_S(E) = t_0 \exp\left(+\frac{\xi}{E}\right) \tag{54}$$

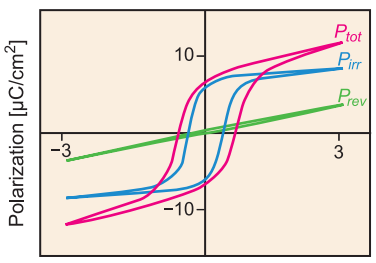

Figure 32: Total, reversible and irreversible contribution to the polarization of a ferroelectric thin film.

where I_0 and t_0 are constants, E is the applied electric field, and ξ can be regarded as the activation field for switching (see Figure 33). At very high electric fields, the **switching time** is better described by

$$t_S(E) = t_0^* \, E^{-n} \tag{55}$$

where n ranges from 1 to 7 for a variety of materials [53]. As expected, the constants that describe the switching process (i.e. ξ and n) depend on temperature. This makes sense since domain wall motion is thermally activated, and poling and switching will be enhanced as the transition temperature is approached. It is also important to mention that ferroelectrics typically do not have well-defined switching fields, so that the amount of polarization switched depends both on the field amplitude, and the length of time the field is applied.

An alternative method of measuring switching is to monitor the current flow as sinusoidal or triangular waveforms are applied. Fundamentally, this measures switching during the traversing of the full hysteresis loop. When the field dependence of the switching is properly accounted for, it is possible to model the data by treating the domain reorientation process as a phase transformation problem, following *Kolmogorov* and *Avrami*. *Ishibashi* included the field dependence of the polarization switching and modelled the *D-E* hysteresis loops in relation to the excitation frequency [54]. While the mathematics here is more complicated, the result can provide considerable insight into the **switching kinetics**. *Ishibashi* has found good agreement of Eq. (55) with experimental data on triglycine sulfate (TGS) single crystals especially the pronounced *frequency dependence of the coercive field*

$$E_c \propto f^{-\beta} \tag{56}$$

This has also been observed for perovskite-type single crystals as shown in Figure 34. A microscopic description of the motional process of ferroelectric domains yields similarities with nucleation phenomena. The switching time for a domain of given size exhibits distinctly different field dependencies in low and high field regimes.

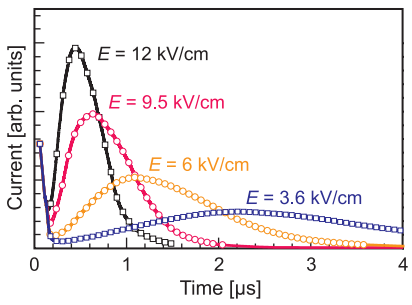

Figure 33: Polarization switching current of TGS single crystal at different electrical fields.

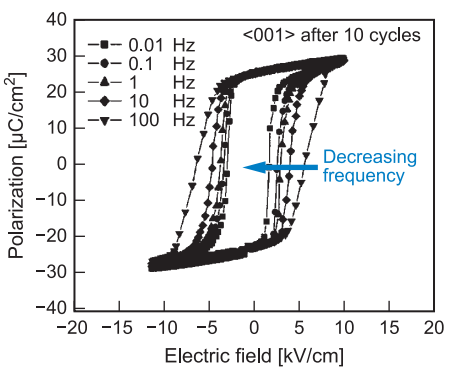

Figure 34: Hysteresis loops at different frequencies of a $[001]_c$-oriented 95.5 % $Pb(Zn_{1/3}\,Nb_{2/3})O_3$-4.5 % $PbTiO_3$ single crystal measured at 10 kV/cm after 10 cycles [55].

5 Optical Properties

Having covered the dielectric and ferroelectric properties of polar dielectrics at low and medium frequencies, in the final section we will now deal with some selected optical properties of polar materials which are important for microwave (see Chap. 36) and photonic (see Chaps. 35) devices. For a deeper insight into the optical properties of matter, the reader is referred to the textbooks [56]–[59].

5.1 Propagation of Electromagnetic Waves in Condensed Matter

The interaction between polar matter and an electromagnetic field results in a **retardation** of the exciting signal. The time delay results in frequency-dependent material properties, while the spatial delay leads to wave-number-dependent ($k = 2\pi/\lambda$) properties, which require a description by an action at a distance theory.

In the following, we will discuss the simplest case where the response of the medium only depends on the fields at neighboring sites. For this case, we derive a wave equation in which the phase velocity c depends on the local material properties. Thus, the frequency ω and the wave number k are not fully independent, but follow from the wave equation as $\omega/k = c$.

We start with **Maxwell's equations** in a medium with free electric charges and currents

$$\begin{aligned} \nabla\times\boldsymbol{H} &= \dot{\boldsymbol{D}} + \boldsymbol{j} \\ \nabla\times\boldsymbol{E} &= -\dot{\boldsymbol{B}} \\ \nabla\cdot\boldsymbol{D} &= \rho_{\text{free}} \\ \nabla\cdot\boldsymbol{B} &= 0 \end{aligned} \tag{57}$$

where $\boldsymbol{D}$ denotes the electric displacement, $\boldsymbol{B}$ the magnetic flux density, $\boldsymbol{E}$ the electric field, and $\boldsymbol{H}$ the magnetic field, $\boldsymbol{j}$ the current density, and ρ_{free} the density of free charges; $\nabla\cdot$ and $\nabla\times$ are the divergence and the curl operations, and the "dot" denotes the time derivative ($\partial/\partial t$).

The relation between the field quantities and the flux densities, which depend on the material properties, is given by the **constitutive equations**

$$\begin{aligned} \boldsymbol{D} &= \varepsilon_0 \boldsymbol{E} + \boldsymbol{P} \\ \boldsymbol{B} &= \mu_0 \left(\boldsymbol{H} + \boldsymbol{M} \right) \end{aligned} \tag{58}$$

where $\boldsymbol{P}$ is the polarization density and $\boldsymbol{M}$ the magnetization density. The constants ε_0 and μ_0 are the electric permittivity and the magnetic permeability of free space, respectively.

In order to derive the **wave equation** for the components of the fields $\boldsymbol{E}$ and $\boldsymbol{H}$, we must first consider the properties of the medium itself which are reflected in the constitutive equations (58). For reasons of simplicity, we will restrict ourselves to non-magnetic media, which means $\boldsymbol{M} = 0$ and $\boldsymbol{B} = \mu_0 \boldsymbol{H}$. The nature of a dielectric medium is exhibited in the relation between the polarization density $\boldsymbol{P}$ and the electric field $\boldsymbol{E}$, where generally $\boldsymbol{P} = \boldsymbol{P}(\boldsymbol{r},t)$ and $\boldsymbol{E} = \boldsymbol{E}(\boldsymbol{r},t)$ are functions of position and time.

For the simplest case of a **dielectric medium**, which is linear, non-dispersive, homogeneous, and isotropic, the relation is given by

$$\boldsymbol{P} = \varepsilon_0 \chi'_\mathrm{e} \boldsymbol{E} \tag{59}$$

where the electrical susceptibility χ'_e is a scalar constant and the vectors $\boldsymbol{P}$ and $\boldsymbol{E}$ are parallel and proportional at any position and time.

A necessary condition for $\boldsymbol{E}$ and $\boldsymbol{H}$ to satisfy Maxwell's equations (57) is that each component satisfies the **wave equation**, which reads for $\boldsymbol{E}$

$$\nabla^2 \boldsymbol{E} - \frac{1}{c^2} \frac{\partial^2 \boldsymbol{E}}{\partial t^2} = 0 \tag{60}$$

In this case, the phase velocity of the electromagnetic wave in the material is given by

$$c = \frac{1}{\sqrt{\varepsilon_0 \mu_0 \cdot \varepsilon'_\mathrm{r}}} = \frac{c_0}{n} \quad \text{with} \quad c_0 = \frac{1}{\sqrt{\varepsilon_0 \mu_0}} \quad \text{and} \quad n = \sqrt{\varepsilon'_\mathrm{r}} \tag{61}$$

Here, c_0 defines the *speed of light* in free space, and n the *refractive index* of the material.

For **inhomogeneous** dielectric media (as for example a graded index medium), the proportionality equation (59) still remains valid, but the material properties are functions of the position: $\chi'_\mathrm{e} = \chi'_\mathrm{e}(\boldsymbol{r})$, $\varepsilon'_\mathrm{r} = \varepsilon'_\mathrm{r}(\boldsymbol{r})$, and $n = n(\boldsymbol{r})$. As long as $\varepsilon'_\mathrm{r}(\boldsymbol{r})$ varies in space at a much slower rate than the field $\boldsymbol{E}(\boldsymbol{r},t)$, the wave equation (60) remains applicable.

In **anisotropic media**, the relation between polarization and electric field depends on the direction of the vector $\boldsymbol{E}$; in particular $\boldsymbol{P}$ and $\boldsymbol{E}$ are not necessarily parallel. In the mathematical formulation, the dielectric properties of the medium are described by a matrix $\{\chi'_{\mathrm{e},ij}\}$ of 3×3 elements known as the *susceptibility tensor*. Correspondingly, ε'_r and n also change into tensors with elements $\{\varepsilon'_{\mathrm{r},ij}\}$ and $\{n_{ij}\}$. As waves with different polarization directions travel at different velocities and undergo different phase shifts, the total polarization vector is changed as the wave propagates through the material. Therefore, anisotropic materials provide useful components of optical devices (see Sec. 5.3.1).

In **dispersive media**, the relation between $\boldsymbol{P}(t)$ and $\boldsymbol{E}(t)$ is governed by a dynamic linear system described by an impulse-response function corresponding to a frequency-dependent susceptibility $\chi_\mathrm{e} = \chi_\mathrm{e}(\omega)$. Consequently, the characteristic quantities $\underline{\varepsilon}_\mathrm{r}$ and $\underline{n}$ become complex. Analogously to the complex permittivity (see Eq. (10)) the **complex refractive index** $\underline{n}$ is divided into the real refractive index n and the absorption index κ

$$\underline{n} = n + i\kappa \tag{62}$$

For non-magnetic media, where $\underline{n} = \sqrt{\underline{\varepsilon}_\mathrm{r}}$, we find for the real and imaginary part of the relative permittivity

$$\varepsilon'_\mathrm{r} = n^2 - \kappa^2 \quad \text{and} \quad \varepsilon''_\mathrm{r} = 2n\kappa \tag{63}$$

These important equations enable the dielectric function to be determined from experimental investigations of the propagation behavior of electromagnetic waves in the material.

In a **non-linear dielectric** medium, the polarization is some non-linear function of the electric field $\boldsymbol{P} = F(\boldsymbol{E})$, as for example given by the most general *Taylor expansion* $\boldsymbol{P} = a_1 \boldsymbol{E} + a_2 \boldsymbol{E}^2 + a_3 \boldsymbol{E}^3$, where a_1, a_2, a_3 are constants. The wave equation (60) is not applicable to electromagnetic waves in non-linear media. Instead, *Maxwell's equations* have to be solved to derive a non-linear partial differential equation for these waves. For non-linear systems the principle of superposition is no longer applicable and optical waves interact with each other.

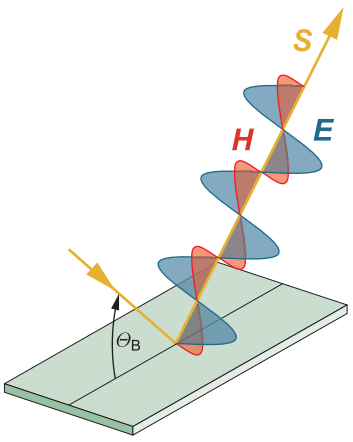

Figure 35: Planes of oscillation of the electrical and magnetic field vectors of linearly polarized light generated by reflection.

5.2 Transmission of Electromagnetic Waves

We will first introduce the most important example of a monochromatic electromagnetic wave – the **plane wave**. Spherical waves and Gaussian beams are other common wave types (see [58]). The medium is assumed to be linear, homogeneous, isotropic, non-dispersive, and non-magnetic according to Sec. 5.1.

We will now consider a monochromatic electromagnetic wave, whose electric and magnetic field components are plane waves of wave vector $\boldsymbol{q}$ as described by $\boldsymbol{E} = \boldsymbol{E}_0 \cdot \exp[i(\boldsymbol{qr} - \omega t)]$. Substituting the corresponding equations for $\boldsymbol{E}$ and $\boldsymbol{H}$ into *Maxwell's equations* (57), we obtain

$$\begin{aligned} \boldsymbol{q} \times \boldsymbol{H}_0 &= -\omega \varepsilon_0 \varepsilon_r' \boldsymbol{E}_0 \\ \boldsymbol{q} \times \boldsymbol{E}_0 &= \omega \mu_0 \boldsymbol{H}_0 \end{aligned} \tag{64}$$

It follows that $\boldsymbol{E}$, $\boldsymbol{H}$, and $\boldsymbol{q}$ are mutually orthogonal. The wave is called a **transverse electromagnetic (TEM) wave**. From a comparison of the two equations in (64), we find the equality $q = \omega/c = n\,\omega/c_0 = n\,q_0$, which is the condition that satisfies the wave equation (60).

The ratio between the amplitudes of the electric and magnetic fields

$$E_0/H_0 = n^{-1}\sqrt{\mu_0/\varepsilon_0} \tag{65}$$

is therefore defined as the impedance of the medium.

The flow of the electromagnetic power which is governed by the complex **Poynting vector**

$$\underline{\boldsymbol{S}} = \tfrac{1}{2}\,\underline{\boldsymbol{E}} \times \underline{\boldsymbol{H}}^* \tag{66}$$

is parallel to the wave vector $\boldsymbol{q}$ (compare with Figure 35; * denotes the complex conjugate). The magnitude of the time-averaged Poynting vector equals the optical intensity of the TEM wave, which is therefore proportional to the squared absolute value of the complex envelope of the electric field

$$I = \left|\boldsymbol{E}_0\right|^2 \cdot n \left(2\sqrt{\mu_0 / \varepsilon_0}\right)^{-1} \tag{67}$$

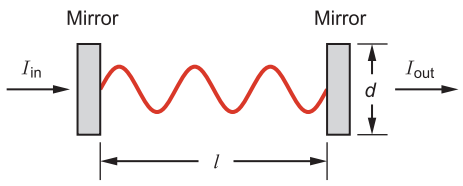

Figure 36: Standing wave inside an optical resonator.

5.2.1 Resonator and Waveguide Modes

In microwave and optical devices (see Chaps. 35 and 36), we have to deal with electromagnetic waves that are amplified in **resonator systems** or guided by means of **wave guides**. As the simplest example, we will briefly discuss the case of a TEM plane wave inside a resonator consisting of two plane-parallel mirrors, as shown in Figure 36. If the diameter d of the mirrors is large compared to their distance l, the resonator is identical to a *Fabry-Perot interferometer* (see [57]). For the frequencies $f_\xi = \xi \cdot c/2l$ ($\xi = 1, 2, 3\ldots$) **standing waves** are obtained between the mirrors. The frequency difference between successive standing waves $\Delta f = f_{\xi+1} - f_\xi = c/2l$ is also called the basic frequency since it is identical to the lowest eigenfrequency of the resonator ($\xi = 1$). The transmission of the interferometer for a plane, perpendicular incident beam of intensity I_{in}, is a function of the frequency f

$$\frac{I_{in}}{I_{out}} \propto \frac{1}{\sin^2\left(2\pi f \cdot l/c\right)} \tag{68}$$

For the resonance frequencies $f_\xi = \xi \cdot c/2l$, the transmission has a maximum value. The standing waves of resonance frequency f_ξ are also called **longitudinal or axial cavity modes**, because the standing waves are set up along the cavity or z-axis, and the resonance frequency only depends on the corresponding number of nodes.

In contrast to the ideal Fabry-Perot interferometer, in practical cavities the assumption of infinitely large mirrors ($d \gg l$) is not valid. In fact, we find the opposite case, namely that the diameter of the front planes (or mirrors) is small compared to the distance ($d \ll l$). The limited dimensions of the mirrors cause a collimation of the ray inside the resonator, thus resulting in diffraction of the wave. This diffraction leads to **transverse modes** which are sustained in the resonator. Since the fields are almost normal to the z-axis they are known as TEM_{mn} modes (transverse electric and magnetic). The m and n subscripts are the integer number of transverse nodal lines in the x- and y-directions across the emerging beam. The form of the different TEM_{mn} modes depends on the shape of mirror (plane or confocal) as well as on the form of its cross section (rectangular or circular). Examples of typical TEM_{mn} mode configurations are shown in Figure 37.

5.2.2 Polarization

The polarization of light is determined by the direction of the electric field vector $\boldsymbol{E}(\boldsymbol{r},t)$. For transverse electromagnetic waves (TEM waves), the electric field vector lies in a plane perpendicular to the propagation direction. Generally, the wave is said to be **elliptically polarized**. When the ellipse degenerates into a straight line or a circle, the wave is said to be **linearly or circularly polarized**, respectively. Figure 35 shows, as an example, the planes of oscillation of the electrical and magnetic field vectors of linearly polarized light generated by reflection.

Polarization plays an important role in the interaction of light with matter, because it is mainly the electrical field vector $\boldsymbol{E}$ that interacts with matter (Sec. 3.2). In the context of optical applications, some important examples are listed below:

- The polarization of the incident beam determines the amount of light reflected at the boundary between two materials.
- Light scattering from matter is polarization-sensitive.
- The refractive index of anisotropic media, and thus the phase velocity and the phase shift of the wave, depend on the polarisation.
- Optically active materials have the ability to rotate the plane of polarization of polarized light.
- The absorption constants of certain materials are polarization-dependent.

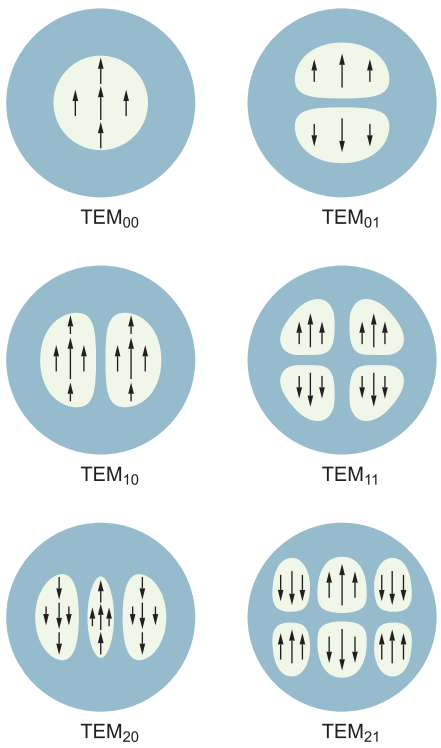

Figure 37: Mode configurations of a confocal optical resonator with rectangular symmetry (after [57]).

5.2.3 Reflection and Refraction

The polarization-dependent reflection and refraction of light at a boundary between two dielectric media is of fundamental importance for the functionality of optical devices. The phenomenon of **total reflection** is the basic principle of light pipes (see Chap. 35).

Here, we will examine the reflection and refraction of a monochromatic plane wave of arbitrary polarization incident at a planar boundary between two dielectric media with refractive indices n_1 and n_2 as depicted in Figure 38. The media are again assumed to be linear, homogeneous, isotropic, non-dispersive, and non-magnetic. Considering the angles of the different beams with respect to the axis of incidence, the following relations hold (see [57]):

- the angle of reflection equals the angle of incidence: $\theta_3 = \theta_1$;
- the angles of refraction and incidence satisfy *Snell's law*: $n_1 \sin\theta_1 = n_2 \sin\theta_2$.

To calculate the **reflection** and **transmission coefficients**, one has to relate the amplitudes and the polarizations of the three waves, taking into account the boundary conditions required by the electromagnetic theory (tangential components of $\boldsymbol{E}$ and $\boldsymbol{H}$ and normal components of $\boldsymbol{D}$ and $\boldsymbol{B}$ are continuous at the boundary; see also [6]). The calculations result in a dependence of the coefficients on the polarization of the incident beam. Therefore, we have to distinguish between a **transverse electric** (TE) field or **s-polarization**, for which the electric fields are orthogonal to the plane of incidence, and a **transverse magnetic** (TM) field or **p-polarization**, where the electric fields are parallel to the plane of incidence.

The resulting expressions for the reflection and transmission coefficients, the **Fresnel equations**, read for *s*-polarisation

$$r_\mathrm{s} = \frac{n_1\cos\theta_1 - n_2\cos\theta_2}{n_1\cos\theta_1 + n_2\cos\theta_2} \quad \text{and} \quad t_\mathrm{s} = 1 + r_\mathrm{s} \tag{69}$$

and for *p*-polarisation

$$r_\mathrm{p} = \frac{n_2\cos\theta_1 - n_1\cos\theta_2}{n_2\cos\theta_1 + n_1\cos\theta_2} \quad \text{and} \quad t_\mathrm{p} = \frac{n_1}{n_2}\left(1 + r_\mathrm{p}\right) \tag{70}$$

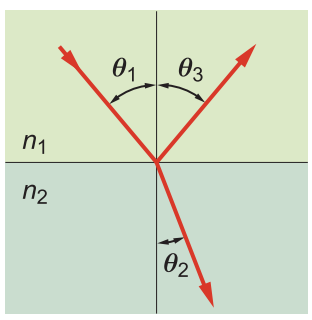

Figure 38: Incident, reflected and refracted beam at the boundary between two dielectric media.

From (70), it follows that the reflection coefficient for a *p*-polarized beam vanishes at a certain angle $\theta_1 = \theta_\mathrm{B}$, the so-called **Brewster angle**, which is given by

$$\tan\theta_\mathrm{B} = \left(n_1/n_2\right) \tag{71}$$

The property that *p*-polarized light is not reflected at the Brewster angle is used for the design of polarizers, so called *Brewster windows*, see Figure 35.

The reflection and transmission coefficients r and t are ratios of the complex amplitudes. The power reflectance R and transmittance T are defined as the ratios of the power flow of the reflected and transmitted wave to that of the incident wave. Thus, we obtain

$$R = |r|^2 \quad \text{and} \quad T = 1 - R \tag{72}$$

5.3 Interaction of Light with Matter

In optical devices various effects are used for guiding and modulating electromagnetic waves. In general, the light wave interacts with the electrons that are bound elastically in the material.

5.3.1 Birefringence

We now deal with the refraction of a plane wave at the boundary between an isotropic medium, as for example air ($n_1 = 1$), and an *anisotropic* medium. For example, $BaTiO_3$ in the tetragonal and the rhombohedral phases is uniaxially birefringent, while the orthorhombic phase exhibits birefringent behavior with two axes. Due to its *optical anisotropy*, the medium supports two modes of distinctly different phase velocities. Therefore, each incident wave gives *two* refracted waves with two different directions and different polarizations (see Figure 39). The effect is called **birefringence**.

As a simple example, we take a uniaxial crystal and a plane of incidence parallel to the optical axis (for further discussions see [58]). The two refracted waves which satisfy the phase-matching condition at the boundary are:

- an **ordinary wave** of orthogonal (s-) polarization at an angle $\theta = \theta_o$;
- an **extraordinary wave** of parallel (p-) polarization at an angle $\theta = \theta_e$.

With respect to optical device applications, anisotropic crystal plates serve as polarizing beam splitters, creating two laterally separated rays with orthogonal polarisations.

5.3.2 Absorption

When we discuss the interaction of electromagnetic waves with matter, we also have to consider the absorption of electromagnetic waves in the dielectric medium which is strongly related to the dielectric properties described by the complex permittivity $\underline{\varepsilon}_r$. In absorbing media, the wave equation (60) remains applicable, but a complex wave number is used to account for the losses

$$\underline{q} = \omega\sqrt{\underline{\varepsilon}_r(\varepsilon_0\mu_0)} = \sqrt{\varepsilon_r' + i\varepsilon_r''}\cdot q_0\,, \quad q_0 = \frac{\omega}{c_0} \tag{73}$$

In terms of the complex refractive index (Eq. (62)), $\underline{q}$ reads

$$\underline{q} = \underline{n}\cdot q_0 = (n + i\kappa)\cdot q_0 \tag{74}$$

For a monochromatic plane wave travelling in $-z$-direction through an absorbing medium

$$\underline{\boldsymbol{E}} = \boldsymbol{E}_0\exp\left[i\left(\underline{q}z - \omega t\right)\right] = \boldsymbol{E}_0\cdot\exp(-\kappa q_0 z)\exp\left[i\left(nq_0 z - \omega t\right)\right] \tag{75}$$

we find a phase velocity of $c = c_0/n$ and an exponentially decaying amplitude.

For the intensity of the transmitted wave we derive the **Lambert-Beer's law**

$$I(z) = I_0\cdot e^{-a\,z} \tag{76}$$

where a is the absorption constant. For weakly absorbing media, we find

$$a(\omega) = \omega\,\varepsilon_r''(\omega)/c_0 \tag{77}$$

Eq. (77) is a particularly simple relation between the empirical absorption constant and the dielectric response function of a system.

5.3.3 The Pockels and Kerr Effects

In certain materials, such as ionic crystals, the positions of the ions and the shapes of the electronic orbitals are distorted when the material is subjected to an electric field (see Sec. 3.2). The ***electro-optical effect*** is the change in the refractive index (caused by a change in the dielectric properties) due to the application of a dc or low-frequency electric field.

The dependence of the refractive index on the applied electric field takes two forms:

- the refractive index changes in proportion to the applied field: $n \propto E$.
  This is called the **linear electro-optical** or the **Pockels effect**. This effect is observed for ferroelectric materials with a preferential axis (see Sec. 4.3).

- the refractive index changes in proportion to the square of the applied field: $n \propto E^2$. This is known as the **quadratic electro-optical** or the **Kerr effect**. This effect is observed for dielectrics (see Sec. 2.3).

The Pockels effect, in particular, is used for many electro-optical devices, for example, phase modulators, switches, spatial intensity modulators, and the Pockels readout optical modulator (PROM) [58].

5.3.4 Photorefractive Materials

Photorefractive materials combine *photoconductive* and *electro-optical* behavior. They are thus able to detect and store spatial optical intensity distributions in the form of spatial patterns of altered refractive index. Photo-induced charges create a space-charge distribution that produces an internal electric field, which, in turn, alters the refractive index due to the electro-optical effect. **Photorefractive** devices therefore permit light to control light [59].

In **photoconductors**, free charge carriers are generated under illumination due to the absorption of photons, and the conductivity increases. In the dark, the electron-hole pairs recombine and the conductivity decreases.

When a **photorefractive material** is exposed to light, free charge carriers are generated by excitation from impurity energy levels to the conduction band, at a rate proportional to the optical power. Carriers diffuse into areas of low intensity where they are trapped by other ionized impurities. The result is an inhomogeneous space-charge distribution generated by a light intensity pattern. The charge distribution creates an internal electric field that modulates the refractive index by the Pockels effect. The image may be accessed optically by monitoring the spatial index pattern with a probe optical wave. The pattern can be erased by illumination or heating of the photorefractive material. Important material candidates are barium titanate ($BaTiO_3$), bismuth silicon oxide, lithium niobate, and also gallium arsenide. The photorefractive effect is the basis for modern holographic storage devices. This is the topic of Chap. 32.

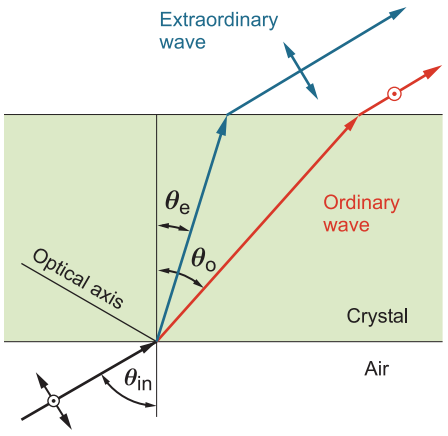

Figure 39: Birefringence through an anisotropic, uniaxial medium.

6 Closing Remarks

This chapter presented a short review of the basic concepts of the interactions between electromagnetic fields and condensed matter. The polarization of the material which interacts with the electric field of the signal wave may be either induced by the electric field, as is the case in dielectrics, or it may be an intrinsic property of the material, as is the case in pyro- and ferroelectric materials. The ability of a crystal to exhibit spontaneous electrical polarization is related to the point group describing the structure and requires a symmetry group with a polar axis.

Among the different dielectrics and ferroelectrics, the perovskites are the most important. Multiple distortions of the cubic perovskite prototype are known, leading to the possibility of multiple phase transitions as a function of temperature, as in barium titanate, or multiple phases as the composition is changed, as in PZT. When morphotropic phase boundaries are present, peaks in the dielectric and piezoelectric properties are typically observed.

The entire spectrum from the dc response to the optical frequencies was covered. The dc response is important for capacitors and electronic devices, permitting the design of capacitors with increased or variable capacitance. The dc and the low-frequency ac response are dominated by displacing charged ions within the material. As a consequence, lattice distortions, vibrations and phonon dynamics play an important role, and sound waves are easily coupled to alternating electrical fields. In ferroelectrics, optical lattice vibrations exist where the differently charged sub-lattices vibrate against each other. In particular for the transverse optical mode at the zone center, the restoring forces for these modes are such that electric Coulomb forces and elastic lattice forces work against each other. As a consequence the transverse optical zone center modes soften. If this compensation effect is complete and Coulomb and elastic forces cancel each other out, then the corresponding phonon condenses out and a ferroelectric displacive phase transition takes place. The underlying lattice vibrations may only be accessed by inelastic neutron spectroscopy, whereas the phonon dispersion relations can be directly measured.

Domains in ferroelectrics are formed in order to minimize the total energy. Thus, the static domain patterns depend on both the electrical and elastic boundary conditions for the system. For any material, the allowed domain variants are controlled by the crystallography of the ferroelectric phase. Domain walls mark the boundaries between domains, and are characterized by the angle between the polarization vectors on either side of the wall. The motion of domain walls is strongly influenced by pinning effects.

At optical frequencies, only the electrons are able to follow the rapid changes of the electrical field, and the ionic lattice provides the background of a periodic static charge distribution. Within a transparent polarizable material, it is the interplay between the asymmetric built-in lattice charge distribution and an intrinsic polarization with the electric field of the propagating electromagnetic wave which acts on the valence electrons of the crystal in a complex and very interesting way, leading to electro-optic effects, acousto-optic devices, nonlinear optics, frequency conversion, and even to holographic storage applications.

Acknowledgments

The editor gratefully acknowledges Sebastian Schmelzer (RWTH Aachen University) for critical review and his helpful suggestions.

References

[1] N. W. Ashcroft, N. D. Mermin, D. Mermin, *Solid State Physics*, Holt, Rinehart and Winston, New York, 1976.

[2] H. Ibach, H. Lüth, *Solid-State Physics: An Introduction to Principles of Materials Science*, Springer, Berlin, New York, 2003.

[3] C. Kittel, *Introduction to Solid State Physics*, John Wiley & Sons, Hoboken, New Jersey, 2005.

[4] O. Madelung, *Introduction to Solid State Theory*, Springer Series in Solid State Sciences, Vol. 2, Springer, Berlin, Heidelberg, New York, 1978.

[5] L. Bergmann, C. Schaefer, *Constituents of Matter: Atoms, Molecules, Nuclei and Particles*, edited by Wilhelm Raith, W. de Gruyter, Berlin, New York, 1997.

[6] R. P. Feynman, *The Feynman Lectures on Physics 'Mainly Electromagnetism and Matter'*, Calif. Addison-Wesley, Redwood City, 1989.

[7] S. M. Sze, *Physics of Semiconductor Devices*, John Wiley & Sons, Hoboken, New Jersey, 2007.

[8] A. J. Moulson and J. M. Herbert, *Electroceramics: Materials, Properties, Applications*, Chapman and Hall, London, New York, 1990.

[9] R. C. Buchanan, *Ceramic Materials for Electronics*, Marcel Dekker, New York, 2004.

[10] B. Jaffe, W. R. Cook Jr., and H. Jaffe, *Piezoelectric Ceramics*, Academic Press, London, New York, 1971.

[11] H. Fröhlich, *Theory of Dielectrics: Dielectric Constant and Dielectric Loss*, Clarendon Press, Oxford, 1986.

[12] A. K. Jonscher, *Dielectric Relaxation in Solids*, Chelsea Dielectrics Press, London, 1983.

[13] M. Born and K. Huang, *Dynamical Theory of Crystal Lattices*, Clarendon Press Oxford, 1988.

[14] R. K. Singh, S. P. Sanyal, *Phonons in Condensed Matter Physics*, Wiley, New York, 1990.

[15] H. Bilz, W. Kress, *Phonon Dispersion Relations in Insulators*, Springer, Berlin, New York, 1979.

[16] L. Brillouin, *Wave Propagation in Periodic Structures*, Dover Publications, New York, 1953.

[17] R. Claus, L. Merten, J. Brandmüller, *Light Scattering by Phonon-Polaritons*, Springer Tracts in Modern Physics, Vol. 75, Springer, Berlin, Heidelberg, New York, 1975.

[18] F. Jona and G. Shirane, *Ferroelectric Crystals*, New York, Dover Publications, 1993.

[19] B. A. Strukov, A. P. Levanyuk, *Ferroelectric Pheonomena in Crystals*, Springer, Berlin, Heidelberg, New York, 1998.

[20] M. E. Lines and A. M. Glass, *Principles and Applications of Ferroelectrics and Related Materials*, Clarendon Press, Oxford, 1977.

[21] B. C. Fraser, H. Danner, R. Papinsky, Phys. Rev. **100**, 745 (1955).

[22] R. E. Newnham, *Structure-Property Relations*, Springer-Verlag, New York, 1975.

[23] B. Jaffe, W. Cook, and H. Jaffe, *Piezoelectric Ceramics*, Academic Press, London, 1971.

[24] J. F. Nye, *Physical Properties of Crystals*, Clarendon Press, Oxford, 1979.

[25] C. Basceri, S. K. Streiffer, A. I. Kingon, R. Waser, J. Appl. Phys. **82**, 2497 (1997).

[26] S. Triebwasser, IBM Jour. Res. Dev. **2**, 617 (1958).

[27] K.-H. Hellwege and A. M. Hellwege, eds., *Complex Perovskite-type Oxides*, Landolt–Börnstein: Oxides, Vol. 16a, Springer-Verlag, 1981.

[28] E. Nakamura and T. Mitsui, ed., *Complex Perovskite-type Oxides*, Landolt–Börnstein: Oxides, Vol. 28, Springer-Verlag, 1990.

[29] B. Noheda, D. E. Cox, G. Shirane, R. Guo, B. Jones, and L. E. Cross, Phys. Rev. B **63**, 014103, (2001).

[30] T. M. Shaw, S. Trolier-McKinstry, and P. C. McIntyre, Annu. Rev. Mater. Sci. **30**, 263 (2000).

[31] N. Pertsev, A. Zembilgotov, A. Tagantsev, Phys. Rev. Lett. **80**, 1988 (1998).

[32] N. Pertsev, A. Zembilgotov, S. Hoffmann, R. Waser, A. Tagantsev, J. Appl. Phys. **85**, 1698 (1997).

[33] W. Cao and L. E. Cross, Phys. Rev. B**44**, 5 (1991).

[34] J. Fousek and V. Janovec, Appl. Phys. Lett. **40**, 135 (1969).

[35] W. Cao and C. Randall, Solid State Communications **86,** 435 (1993).

[36] G. Arlt, D. Hennings, G. de-With, J. Appl. Phys. **58**, 1619 (1985)

[37] G. A. Rossetti, L. E. Cross, K. Kushida, Appl. Phys. Lett. **59**, 2524 (1991).

[38] S. K. Streiffer, C. B. Parker, A. E. Romanov, M. J. Lefevre, L. Zhao, J. S. Speck, W. Pompe, C. M. Foster, G. R. Bai, J. Appl. Phys. **83**, 2742 (1998).

[39] K. J. Choi, M. Biegalski, Y. L. Li, A. Sharan, J. Schubert, R. Uecker, P. Reiche, Y. B. Chen, X. Q. Pan, V. Gopalan, L. Q. Chen, D. G. Schlom, C. B. Eom, Science **306**, 1005 (2004).

[40] K. Nashimoto, D. K. Fork, and G. B. Anderson, Appl. Phys. Lett. **66**, 822 (1995).

[41] K. Nagashima, M. Aratani, H. Funakubo, J. Appl. Phys. **89**, 4517 (2001).

[42] B. A. Tuttle et al., in *Science and Technology of Electroceramic Thin Films,* ed. O. Auciello, R. Waser, Kluwer Academic Publishers, 1995.

[43] A. Roelofs, N. A. Pertsev, R. Waser, F. Schlaphof, L. M. Eng, C. Ganpule, V. Nagarajan, R. Ramesh, Appl. Phys. Lett. **80**, 1424 (2002).

[44] A. Roelofs, T. Schneller, K. Szot, R. Waser, Appl. Phys. Lett. **81**, 5231 (2002).

[45] T. Tybell, C. H. Ahn, J. M. Triscone, Appl. Phys. Lett. **75**, 856 (1999).

[46] V. Nagarajan, A. Roytburd, A. Stanishevsky, S. Prasertchoung, T. Zhao, L. Chen, J. Melngailis, O. Auciello, R. Ramesh, Nature Materials **2**, 43 (2003).

[47] S. Chikazumi and S. H. Charap, *Physics of Magnetism*, Krieger Pub Co, 1978.

[48] T. J. Yang, V. Gopalan, P. J. Swart, and U. Mohideen, Phys. Rev. Lett. **82**, 4106 (1999).

[49] O. Boser and D. N. Beshers, Mat. Res. Soc. Symp. Proc.**82**, 441 (1987).

[50] O. Lohse, D. Bolten, M. Grossmann, R. Waser, W. Hartner, G. Schindler, Mater. Res. Soc. Proc. **267**, (1998).

[51] D. Bolten, O. Lohse, M. Grossmann, R. Waser, Ferroelectrics **221**, 251 (1999).

[52] W. J. Merz, Physical Review **95**, 690 (1954).

[53] L. E. Cross, in Encyclopedia of Chemical Technology 10, ed. Kirk Othmer, Wiley, 1980.

[54] S. Hashimoto, H. Orihara, Y. Ishibashi, J. Phys. Soc. Jpn. **63**, 1601 (1994).

[55] M. Ozgul, S. Trolier-McKinstry, C. A. Randall, J. Appl. Phys. **95**, 4296 (2004).

[56] L. Bergmann, C. Schaefer, *Optics of Waves and Particles*, edited by Heinz Niedrig, W. de Gruyter, Berlin, New York, 1999.

[57] E. Hecht, *Optics*, Addison-Wesley Pub. Co., Reading Mass., 2001.

[58] B. E. A. Saleh, M. C. Teich, *Fundamentals of Photonics*, Wiley, New York, 1991.

[59] J. Feinberg, *Photorefractive Nonlinear Optics*, Physics Today (1988).